Assessing the Effects of Fjord Geometry on Greenland Tidewater Glacier Stability

Journal:	*Journal of Glaciology*
Manuscript ID	JOG-23-0087.R1
Manuscript Type:	Article
Date Submitted by the Author:	n/a
Complete List of Authors:	Fischer, Elizabeth; University of Alaska Fairbanks, Geophysical Institute Aschwanden, Andy; University of Alaska Fairbanks, Geophysical Institute
Keywords:	Glacier calving, Climate change, Glacier modelling, Ice velocity, Remote sensing
Abstract:	Tidewater glaciers advance and retreat in unpredictable ways, complicating the task of forecasting the evolution of individual glaciers and the overall Greenland Ice Sheet, much of which is drained by tidewater glaciers. Past observational research has identified a set of processes collectively known as the Tidewater Glacier Cycle (TGC) to describe tidewater glacier evolution in four stages: the advancing stage, the extended stage, the retreating stage and the retreated stage. Once glacier retreat is initiated, the TGC is thought to depend largely on the glacier's calving rate, which is controlled by fjord geometry. However, there has been little modeling or systematic observational work on the topic. Measuring calving rates directly is challenging and thus we developed an averaged von Mises stress state at the glacier terminus as a calving rate proxy that can be estimated from surface velocities, ice thickness, a terminus position, and subglacial topography. We then analyzed 44 tidewater glaciers in Greenland and assessed the glaciers current state in the TGC. Of the 44 glaciers, we find that fjord geometry is causing instability in 10 cases, vs. stability in 7, with 11 in rapid retreat and 16

	have been historically stable.

Assessing the Effects of Fjord Geometry on Greenland Tidewater Glacier Stability

Elizabeth FISCHER,[1] Andy ASCHWANDEN[1]

[1] *Geophysical Institute, University of Alaska Fairbanks, Fairbanks, AK, US*

Correspondence: Elizabeth Fischer <eafischer2@alaska.edu>

ABSTRACT. Tidewater glaciers advance and retreat in unpredictable ways, complicating the task of forecasting the evolution of individual glaciers and the overall Greenland Ice Sheet, much of which is drained by tidewater glaciers. Past observational research has identified a set of processes collectively known as the *Tidewater Glacier Cycle* (TGC) to describe tidewater glacier evolution in four stages: the *advancing stage*, the *extended stage*, the *retreating stage* and the *retreated stage*. Once glacier retreat is initiated, the TGC is thought to depend largely on the glacier's calving rate, which is controlled by fjord geometry. However, there has been little modeling or systematic observational work on the topic.

Measuring calving rates directly is challenging and thus we developed an averaged von Mises stress state at the glacier terminus as a calving rate proxy that can be estimated from surface velocities, ice thickness, a terminus position, and subglacial topography. We then analyzed 44 tidewater glaciers in Greenland and assessed the glaciers current state in the TGC. Of the 44 glaciers, we find that fjord geometry is causing instability in 10 cases, vs. stability in 7, with 11 in rapid retreat and 16 have been historically stable.

1. INTRODUCTION

It has long been known that tidewater glaciers advance and retreat out of sync with land terminating glaciers and external ocean and climate forcing (Post, 1975; Meier and Post, 1987; Pfeffer, 2003). This observation has led to the formulation of the *Tidewater Glacier Cycle* (TGC) (Pfeffer, 2007; Pollard and DeConto, 2009; Brinkerhoff and others, 2017; Post and others, 2011), a combination of processes that proceed in four archetypal phases, as described in Brinkerhoff and others (2017). In the advancing stage, development and advection of a shoal at the front reduces calving and submarine melting, causing glacier thickening and advance. Eventually the glacier enters an extended phase, in which accumulation and ablation are in balance and further advance is halted. A glacier enters the retreating phase when it can no longer maintain sufficient thickness to remain grounded on the shoal and the glacier retreats into progressively deeper water; at which point dramatic unstable rapid retreat takes place. Retreat ends when the terminus approaches a position that reduces the calving in the absence of sedimentation; possibly at a *pinning point* (temporary narrowing of the fjord), or else the terminus effectively re-grounds on bedrock. Multi-decadal modeling studies with sedimentation are able to reproduce this cycle (Nick and others, 2007; Amundson, 2016; Brinkerhoff and others, 2017) even in the absence of variations in climate (Brinkerhoff and others, 2017).

Typical timescales and rates of advance / retreat for tidewater glaciers is an area of active research. Catania and others (2018) report rates of retreat for Greenland tidewater glaciers of up to $500\,\mathrm{m\,a^{-1}}$. Brinkerhoff and others (2017) shows a simulated retreat phase lasting about 100 years and advance phase about 1000 years with the terminus advancing or retreating about 5 km in that time ($50\,\mathrm{m\,a^{-1}}$ retreat and $5\,\mathrm{m\,a^{-1}}$ advance). Carlson and others (2017) reports the Columbia Glacier in Alaska has retreated approx. 20 km in 30 years ($667\,\mathrm{m\,a^{-1}}$). Pearce and others (2022) reports an advance rate of Kangiata Nunaata Sermia of $115\,\mathrm{m\,a^{-1}}$ during the Little Ice Age (12th and 13th centuries CE). In general, the retreat phase of the TGC is thought to happen on a decadal or centennial timescale, and the advance phase is about an order of magnitude slower.

In this observational study, we focus on detecting glaciers beginning, sustaining or finishing the retreat phase using the ITS-LIVE dataset from 1985 through 2018, or 33 years (Gardner and others, 2019). We use *annual* terminus positions, thereby sidestepping the complex issue of seasonal variability. Our timeseries are not long enough to investigate the advance phase. Sedimentation is an important part of the TGC at

the century time scale (Brinkerhoff and others, 2017); but one we can safely ignore in this study covering rapid retreat of numerous glaciers over a few decades.

Interestingly, the TGC suggests that tidewater glacier termini can only remain in stable equilibrium, neither advancing or retreating, at places where further advance would cause a negative feedback: at fjord mouths, at *pinning points* (temporary narrowing of the fjord), and at other places involving change in the fjord width (Mercer, 1961).

Greenland's outlet glaciers are currently at diverse stages in the tidewater glacier cycle. For example, after advancing 800 m from 1973 to 2000, Sermeq Silarleq in central west Greenland retreated 5 km from 2000 through 2019; but just 47 km to the south, Store Glacier has remained remarkably stable during the same time frame (Cheng and others, 2021b).

Many glaciers around Greenland have been retreating since 2000 (Murray and others, 2015), suggesting that conditions required for TGC advance are currently rare. While the TGC has been used as a post-hoc explanation for advancing (McNeil and others, 2021) and retreating glaciers, it has not been used to systematically investigate how a glacier's current behavior reflects the TGC phases. Quantifying where a glacier currently falls in the TGC could help to understand how it might respond to future environmental change.

1.1. Basics of Advance and Retreat

Wood and others (2021) present a model across Greenland in which the position L of a tidewater glacier's grounded terminus is a result of four competing processes causing advance or retreat: advection of ice downstream (q_f) leads to terminus advance, whereas frontal melt (q_m), calving (q_c) and thinning-induced retreat (q_s) (Felikson and others, 2017) lead to terminus retreat. Adopting the convention that positive sign means advancing terminus for all advance/retreat rates (units $\mathrm{m\,s^{-1}}$), mass balance at the ice front requires:

$$\Delta L = L - L_0 = \int_{t_0}^{t} (q_f + q_m + q_c + q_s)\,\mathrm{d}t, \tag{1}$$

where L is the current terminus position, L_0 is the terminus position at a reference time t_0 and t is the current time. The supplement from Wood and others (2021) shows that q_s is at least an order of magnitude smaller than q_c for the glaciers in this study, and we can therefore ignore it. Wood and others (2021) observe or model all the terms of Equation 1 *except* for q_c.

Wood and others (2021) use a parameterization for frontal melt, similar to Slater and others (2019), in which sugblacial discharge and thermal forcing are both derived from an ensemble of *MITgcm* runs (Rignot and others, 2016; Xu and others, 2013): because ocean grid cells are too large to resolve fjords, model-based ocean temperatures at the mouth of each fjord are translated into temperatures inside the fjord at the calving front.[1] Thinning-induced retreat q_s is calculated using a simple, geometrically derived relationship for grounding line migration rate as a function of surface elevation change (Thomas and Bentley, 1978).

Disregarding frontal melt for a moment, stability may be investigated systematically by evaluating the relationship between terminus position and calving rate q_c for each glacier. If a currently stable glacier is about to enter the retreat phase of the TGC, then q_c would be expected to increase as the glacier begins to retreat, potentially leading to runaway retreat; whereas if the glacier is stabilizing, q_c would be expected to decrease as the glacier retreats, causing retreat to slow. One could identify glaciers that are about to enter or exit the rapid retreat phase of the TGC by investigating the correlation between observed changes in q_c versus observed changes in terminus position.

Measuring or modeling all four components of Equation 1 individually would allow us to do just that. However, such observations are challenging because of limitations in observational capabilities and uncertainties in process models. While calving rates can be measured with localized systems (Taylor and others, 2022; Walter and others, 2020), earth observing satellites do not provide high enough resolution in time to apply these techniques over a wide region. For this reason, a proxy $\bar{\sigma}_T$, representing relative levels of expected q_c and computable from remote sensing data, is used to evaluate glacier stability instead of the calving rate q_c. This proxy relies on the *von Mises* calving law (von Mises, 1913; Morlighem and others, 2016) as a simple but reasonable model for tidewater glaciers (Section 4.1).

Even with a reliable proxy for q_c, efforts to find a relationship between q_c and observed retreat ΔL will fail: due to warming in the ocean around Greenland, frontal melt has recently become the dominant process driving retreat (Slater and others, 2019; Wood and others, 2021), with calving playing a secondary role. Most glaciers are retreating, and we cannot immediately conclude that observed retreat is due to tidewater glacier instability. Some glaciers continue to retreat even as they move into shallower water, for example Lille Glacier (Figure 15). In order to observe a correlation between glacier retreat and calving rate, it is first necessary to estimate and remove the amount of retreat caused by changes in frontal melt rate q_m. We use the model of Slater and others (2019) for that task.

[1]See section titled *Thermal forcing* in Wood and others (2021), page 8 of 10.

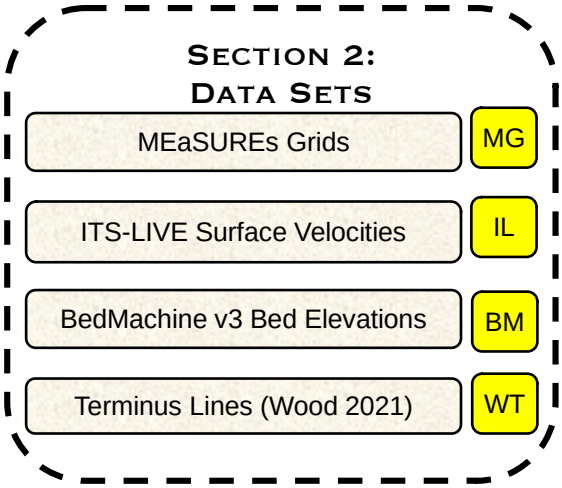

Fig. 1. Data sets used in this study. Each data set is represented by a yellow tag, used in Figure 2. See Section 2 for further details.

1.2. Methodology

We develop an averaged proxy $\bar{\sigma}_T$ for the calving rate q_c, which can be computed from readily-available observations of surface velocities, ice thickness, a terminus line and subglacial topography. The proxy is derived from the *von Mises* calving law (von Mises, 1913; Morlighem and others, 2016), which this study shows in Section 5 can be tuned to be consistent with observations.

Values of $\bar{\sigma}_T$ and L in the recent history of the glacier are regressed against each other, allowing diagnosis of the glacier's stability and current stage in the TGC. In this study we use *annual* averages of L, thereby sidestepping issues of seasonal melting driven by submarine discharge; and we also remove the dominant effects of ocean warming. If $\bar{\sigma}_T$ is found to *decrease* as the glacier retreats, then the fjord geometry at that point in space is destabilizing, providing evidence that the glacier may be entering the retreat phase of the TGC; whereas if $\bar{\sigma}_T$ *increases* the opposite is true and the fjord geometry is now stabilizing the glacier, suggesting the glacier may be finishing the retreat phase of the TGC and moving up onto land.

If $\bar{\sigma}_T$ remains the same as the glacier retreats, the glacier may be retreating through a section of the fjord with nearly constant cross sectional width and depth, typical for glaciers in the middle of rapid retreat. Finally, some glaciers have remained stable in recent years and it is not possible to tell strictly from observations whether $\bar{\sigma}_T$ would go up or down if the terminus were to retreat.

1.3. Paper Overview

The methods in this paper involve an existing set of grid definitions, four datasets, three theoretical models, and 8 interconnected computational / statistical procedures to produce two final results: a classification of

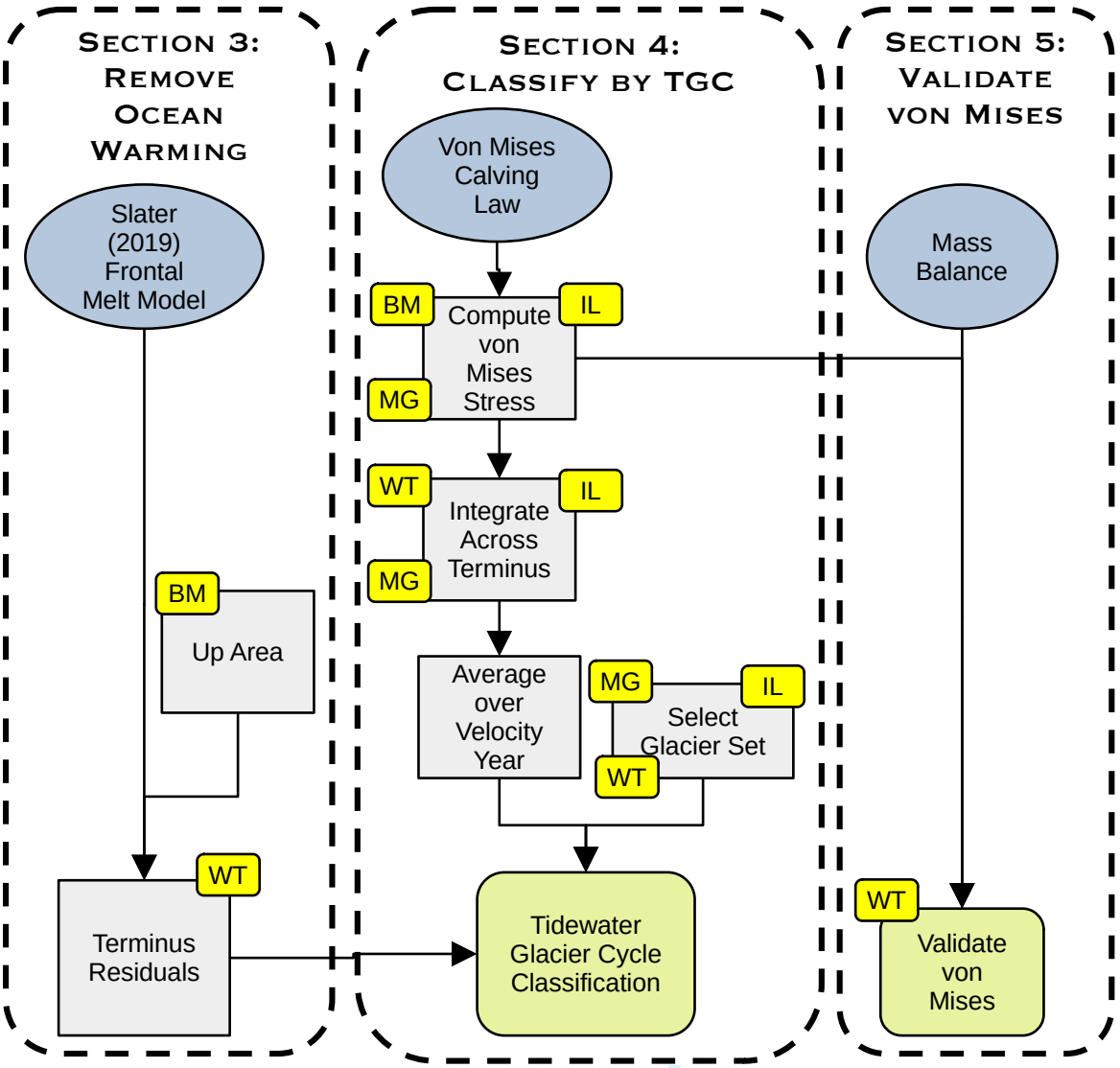

Fig. 2. Models and methods used in this paper: blue ovals are theoretical models, grey rectangles are methods; and green rounded rectangles are methods that produce an end result of this study. Arrows represent dependencies, for example *Up Area* values (Section 3.2) are required to produce *Terminus Residuals*. Section 3 presents the frontal melt model by Slater and others (2019) driven by ocean warming, and uses it to remove effects of ocean warming from terminus data, resulting in terminus residuals. Section 4 introduces the von Mises Calving Law and derives $\bar{\sigma}_T$, a proxy for calving rate, which it regresses against terminus residuals to provide diagnostics on tidewater glaciers. Section 5 uses the data to show why the von Mises calving law is a reasonable model.

glaciers based on their current stage in the TGC, and validation that the von Mises calving criterion is a reasonable model. The models and methods required to attain these conclusions have complex interdependencies, illustrated in an organizational chart in Figure 2 and supported by datasets in Figure 1. Because of these interdependencies, there is no single obvious way to order them. We have ordered sections

Introduction	
σ_T	Average von Mises stress across a glacier terminus T
$\bar{\sigma_T}$	Average of σ_T for one terminus T over different years' velocity fields
L	Generic scalar terminus position
q_f	Rate of advection of ice downstream (positive number)
q_c	Rate of calving (negative number)
q_m	Rate of frontal melt (negative number)
q_s	Rate of thinning-induced retreat (negative number)
Model of Slater and others (2019)	
Q	Subglacial discharge due to surface meltwater runoff and basal melt
TF	Thermal forcing in the fjord
l_s	Observed scalar terminus position
l_p	Modeled scalar terminus position
$l_p = \kappa q_m + \beta$	Empirical predictive relationship for l_p based on $q_m = Q^{0.4}\text{TF}$
Measurement of Terminus	
A_T	Area of fjord upstream of terminus T
$A_T = wl_s + b$	Empirical relationship between A_T and l_s
$l_\epsilon = l_p - l_w$	Terminus residual of observations vs. Slater and others (2019) model
$\vec{n}$	Unit normal to terminus line
Von Mises Model	
$\tilde{\sigma}$	Scalar von Mises tensile stress
$\vec{i}$	Vertically averaged horizontal surface velocity of a glacier
$\dot{\epsilon}$	Strain rate tensor
$\tilde{\dot{\epsilon}}$	Scalar tensile strain rate (Morlighem and others, 2016)
$\dot{\epsilon}_1$, $\dot{\epsilon}_2$	Eigenvalues of $\dot{\epsilon}$
σ	Deviatoric (shear stress) tensor where $\dot{\epsilon} = \tilde{A}\sigma^n$
$\tilde{A}$	Temperature-dependant rate factor with units $\text{s}^{-1}\text{Pa}^{-n}$
$\tilde{B} = \tilde{A}^{-1/n}$	Ice hardness (Greve and Blatter, 2009)
n	Constitutive relation exponent typically assumed to be 3 (Behn and others, 2021)
σ_{max}	Ice yield strength (kPa)
Calving vs. Retreat	
$\Delta l_\epsilon = \nu \Delta \bar{\sigma_T}$	Empirical relationship between l_ϵ and $\bar{\sigma_T}$, disregargin the y-intercept.
R^2	Amount of variance in l_ϵ explained by model
p	Goodness of fit for model
Validation of von Mises Calving	
$L - L_0$	Change in terminus position between reference time t_0 and current the time t
dL/dt	Rate of terminus advance or retreat
Line Integrals on a Grid	
A, B	Two adjacent gridcells covered in ice
u, v	x and y components of horizontal vertically averaged ice velocity
m	A mask identifying gridcells with west-to-east (or south-to-north) flux

Fig. 3. Symbols used in this paper, organized by section where they are introduced.

such that later material builds on earlier material; however, the reader may wish to read the sections in a different order, depending on their interests.

Figure 3 lists all symbols used in this paper. Based on Figure 2, the rest of this paper is organized as follows: Section 2 presents the four datasets used in this study, which are used by the methods in future sections. Section 3 presents the frontal melt model of Slater and others (2019), and describes its use to remove the effects of frontal melt from the terminus data of Wood and others (2021), resulting in *terminus residuals*. Section 4 presents the von Mises calving law (von Mises, 1913; Morlighem and others, 2016; Choi and others, 2018); and presents a series of steps that, when combined with the terminus residuals of Section 3, allow for classification of glaciers within the TGC. Section 6, along with the Supplement, shares

results. Section 7 and Section 8 synthesize and discuss the results further. Finally, Appendix A documents a novel numerical technique, developed in conjunction with this study, that may be applicable for other projects.

2. DATA SETS

We used the following grids and data sets. The reader may wish to skip to Section 3 and refer back to this section as needed.

Local MEaSUREs Grids: Local grids (resolution and extent), as defined by the *MEaSUREs Greenland Ice Velocity* dataset NSIDC-481 (Joughin and others, 2010, 2020), which we re-use for our analysis.

ITS-LIVE Surface Velocities: Annual average surface velocities (advection rate) from 1985 through 2018, necessary to compute the von Mises stress, were obtained from the ITS-LIVE dataset (Gardner and others, 2019) and regridded to the local MEaSUREs grids.

BedMachine v3 Subglacial Topography: Subglacial topography required for this computation was provided by BedMachine v3 (Morlighem and others, 2017) and regridded to the local MEaSUREs grids.

Terminus Lines: The scalar terminus positions of Slater and others (2019) are cross-referenced against information obtained from the two-dimensional terminus lines of Wood and others (2021).

Modeled Frontal Melt: The models of Slater and others (2019) are used to predict frontal melt based on ocean warming.

Selection of Glacier Set: We used glaciers present in the datasets provided by *three* previous studies: Slater and others (2019), Wood and others (2021), Gardner and others (2019); and falling within grids from Joughin and others (2010).

Those datasets are further examined below.

2.1. Local MEaSUREs Grids

The *MEaSUREs Greenland Ice Velocity* dataset NSIDC-481 (Joughin and others, 2010, 2020) has already been constructed to cover many Greenland glaciers, with local high-resolution grids defined in areas with glacier activity (Figure 4). Regridding the other datasets (below) to these local grids allows for detailed

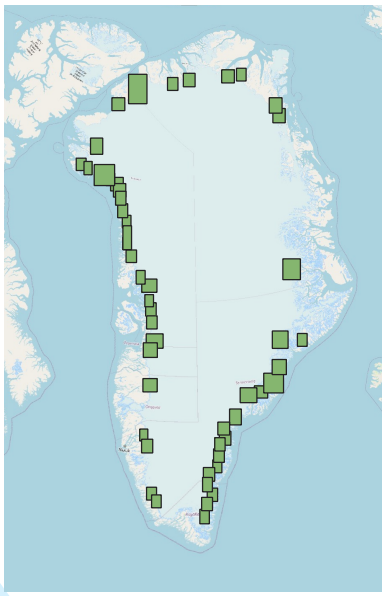

Fig. 4. Local high-resolution grids (green rectangles) defined by the MEaSUREs dataset, NSIDC-0481.

study of individual glaciers while omitting most of the interior of the ice sheet. They also allow for cross-referencing with other datasets and studies that also use the same grids.

Each glacier in our analysis was identified as falling on a single local grid from NSIDC-481 (a *MEaSUREs grid*). For glaciers located on more than one MEaSUREs grid, the most appropriate grid for that glacier was determined by hand based on the distance from the center of the grid for each glacier. Glaciers that did not fall within a MEaSUREs grid were removed from the selection.

2.2. ITS-LIVE Surface Velocities

Annual average surface velocities (advection rate) from 1985 through 2018, necessary to compute the von Mises stress, were obtained from the ITS-LIVE dataset (Gardner and others, 2019), and regridded to the local MEaSUREs grids. An annually averaged dataset was used to avoid complexities of seasonality, surges and short-term variability; however, use of a higher temporal resolution dataset for surface velocities might produce improved statistical precision. Mouginot and others (2017) also provide surface velocity datasets derived from satellite InSAR or optical images, which might be useful in similar future studies, for example in Antarctica.

2.3. BedMachine v3 Subglacial Topography

Subglacial topography required for this computation was provided by BedMachine v3 (Morlighem and others, 2017) and regridded to the local MEaSUREs grids. BedMachine was chosen as our best

understanding of the bed underneath the Greenland Ice Sheet, given available data and models. Knowledge of the bed is typically least certain near each glacier terminus.

2.4. Terminus Lines

Terminus positions may be computed from satellite images by tracing the terminus, either manually (Wood and others, 2021) or via machine learning (Cheng and others, 2021a; Goliber and others, 2022), with newer machine-learning approaches greatly expanding the quantity of available terminus traces. Wood and others (2021) provide one of the two main theoretical models for this study (Section 1.1), and we re-use terminus traces from it to maintain compatibility.

Slater and others (2019) provide the other main theoretical model for this study, but it represents terminus positions as a one dimensional scalar distance up the fjord. This implicitly assumes a specific model of a fjord as a long narrow channel with length much greater its approximately uniform width, which is not always reasonable. There is no simple automated way to delineate center lines, and some fjords have complex geometry not well described by a simple one dimensional model.

Therefore, spatial analysis in this study is conducted on a full two dimensional map of the fjord. For compatibility, the scalar terminus positions of Slater and others (2019) are cross-referenced against information obtained from the two-dimensional terminus lines of Wood and others (2021).

2.5. Modeled Frontal Melt

We use two data sets from Slater and others (2019): annual scalar terminus positions l_s and annual frontal melt rate q_m, modeled as $q_m = Q^{0.4}\mathrm{TF}$, where Q is subglacial discharge due to surface meltwater runoff and basal melt and TF is the thermal forcing in the fjord. These values are based on model ocean outputs of *MITgcm* (Adcroft and others, 2004). The model of Slater and others (2019) may significantly underesimate submarine melting (Sutherland and others, 2019; Catania and others, 2020; Jackson and others, 2022); but at first order we do not expect that to affect results because frontal melt is empirically calibrated to observations (section 3.1).

2.6. Selection of Glacier Set

As described above, this study uses models from Slater and others (2019), data from Wood and others (2021) and Gardner and others (2019), and grids from Joughin and others (2010). Therefore glaciers need to be present in *all four* datasets, resulting in a set of 44 glaciers available for the study as shown in the results (Fig. 5). Although this procedure reduces the number of glaciers for analysis, it maximizes the

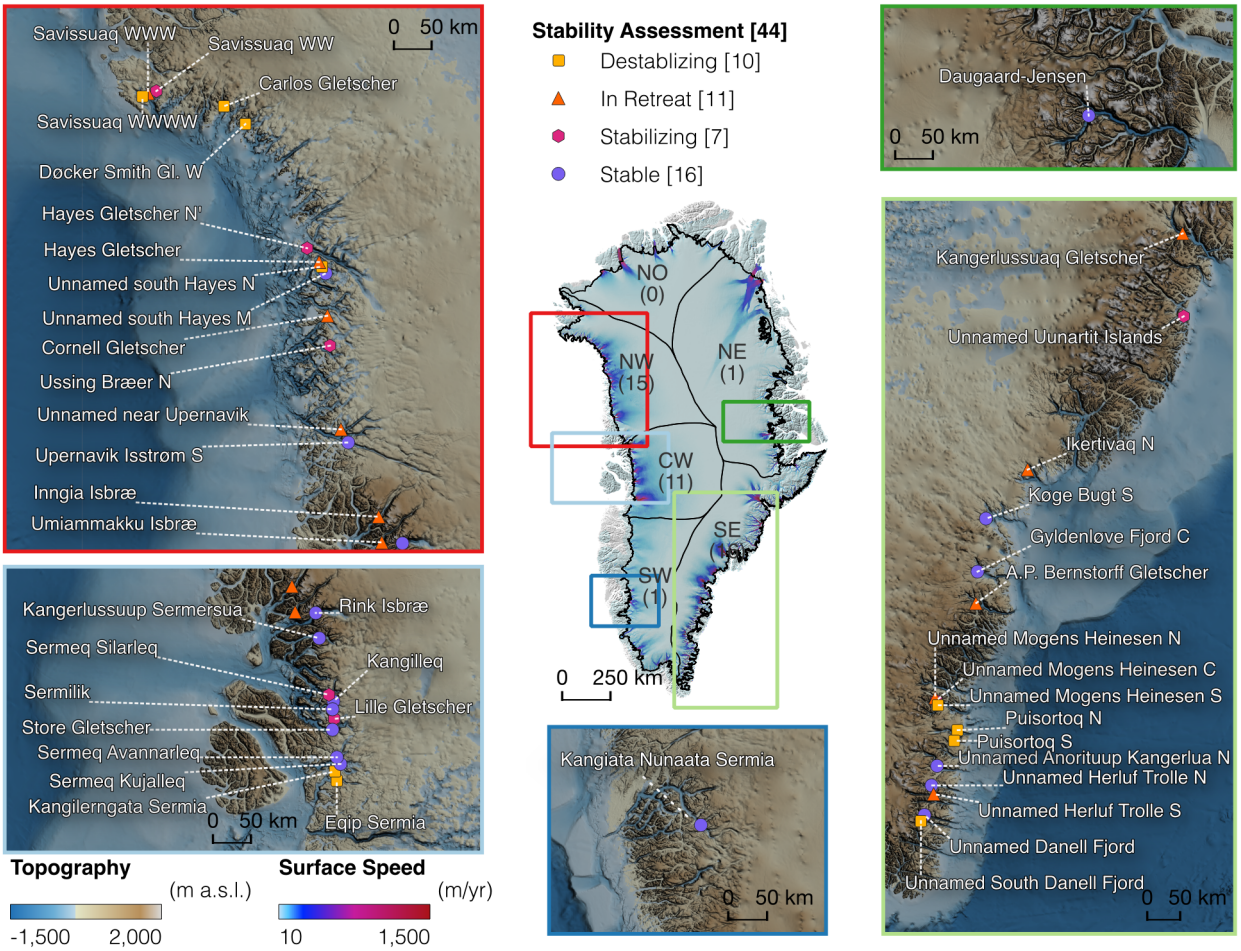

Fig. 5. Location and stability assessment of the 44 Greenland tidewater glaciers in this study. Of the 44 glaciers, 9 glaciers are stable, 7 are stabilizing, 13 are destabilizing, and 15 are in retreat. Subglacial topography is from BedMachine v3 (Morlighem and others, 2014) and surface speeds from ITS-LIVE (Gardner and others, 2019).

ability to compare and cross-reference results with previous studies. Geographic representation of glaciers, classifying by regions as defined by Wood and others (2021), is: central-west Greenland (11 of 14 total tidewater glaciers), north-east (1 of 14), north-west (15 of 64), south-east (16 of 56), and south-west (1 of 12). This study has no geographic representation in the central-east (35 total) or north (12 total) regions of Greenland.

We note that the data sets we used do not include many glaciers in the south-west of Greenland.

3. FRONTAL MELT

3.1. Frontal Melt Model

Slater and others (2019) state that warming oceans are currently the primary driver of tidewater glacier retreat in Greenland. Based on data, they provide a glacier-by-glacier relationship between the change of the scalar terminus position l_p and frontal melt rate q_m, i.e. they empirically derive κ and β, based on data *averaged over 5-year intervals* such that:

$$l_p = \kappa q_m + \beta. \tag{2}$$

This relationship is based on *the process of ice front undercutting / frontal melt only*, modeled because it cannot be observed directly via remote sensing. The value $q_m = Q^{0.4}\mathrm{TF}$ from Slater and others (2019) represents the ocean heat available to drive melting. As a proxy for subglacial discharge Q, Slater and others (2019) used surface meltwater runoff estimated by the regional climate model RACMO2 (Noël and others, 2018); and for TF, they used the monthly EN4 dataset from the Hadley Center consisting of observed subsurface ocean temperature and salinity profiles (Good and others, 2013).

The linear model of Slater and others (2019) incorporates frontal melt from ocean warming but ignores the calving effects due to glacier geometry. Glaciers close to each other will experience similar changes in ocean temperature, but different fjord geometry could cause them to behave differently in spite of similar ocean forcing. Therefore, the model can predict advance or retreat of glaciers as a whole within a region due to ocean warming, but cannot predict the behavior of individual glaciers, which also depends on fjord geometry.

In recent years, ocean warming has become the dominant process causing glaciers in this study to retreat (Slater and others, 2019; Wood and others, 2021). In order to study the secondary effect of fjord geometry, the effects of the dominant process must first be removed from the data. We use the model of Slater and others (2019) to estimate the amount of retreat caused by ocean warming and subtract that out of the total retreat, leaving a *terminus residual* (Section 3.3) in which retreat due to calving is the dominant process.

3.2. Up Area

Spatial analysis in this study is conducted on a full two dimensional map of the fjord. In place of a scalar terminus position L, the scalar *up area* A_T is used, defined as the entire ice-covered area upstream of the glacier terminus T for which the basal topography is below sea level. This avoids assumptions about fjords, their linear geometry or center lines.

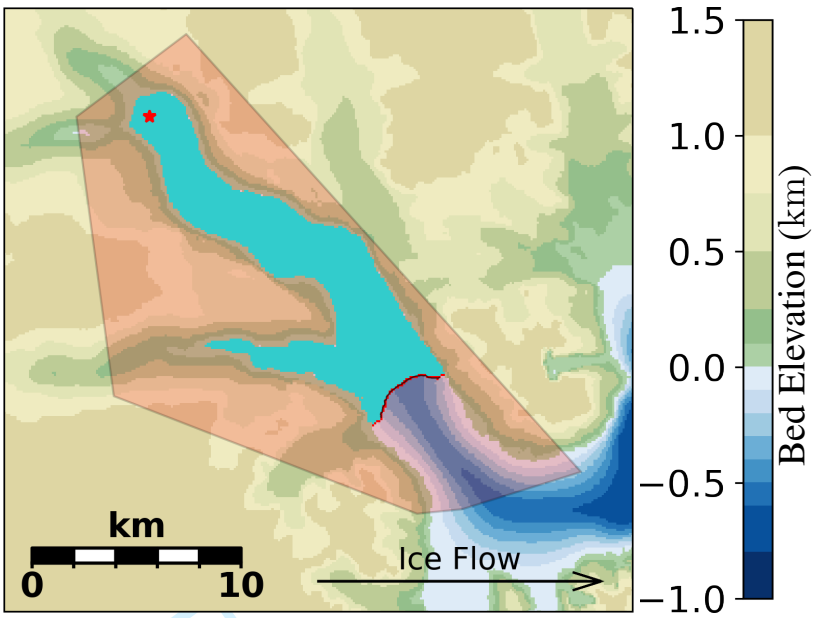

Fig. 6. Aerial map of AP Bernstorff Glacier in Southeast Greenland, with terminus as of year 2005. Digitized terminus datasets typically come in vector format (black line on top of red gridcells), which is rasterized (red grid cells). To help the computer determine the extent of the fjord, we drew a rough polygon around the fjord by hand (red shaded area), and identified a point (red star) that is upstream of *all* expected termini used in this study. Based on these inputs and bathymetry from BedMachine, the computer was able to delineate the extent of the fjord (green) as those gridcells that are below sea level and reachable from the identified point via flood fill.

The up area is calculated as follows (Figure 6). Using GIS software, a polygon is drawn around the fjord by hand, and a single point identified in the upper reaches of the fjord (the *up point*). The fjord is determined in raster form by identifying gridcells within the polygon with bed below sea level. The terminus line is extended to the full width of the fjord and rasterized, to produce the set of gridcells *on* the terminus. A raster *flood fill* algorithm is then used, starting from the up point, to identify all the grid cells of the fjord that are upstream of the terminus. The *up area* is computed by summing the areas of these upstream grid cells.

Because of the way polygons are drawn, A_T does not include far-upstream areas of some fjords. Therefore, *up area* may be used for relative comparison between termini, but not as an absolute measure of how much fjord "remains" ice covered before a glacier becomes land terminating.

3.3. Terminus Residuals

We examine the relationship between fjord geometry and glacier retreat due to calving rates, an effect that Slater and others (2019) determined to be secondary to ocean warming. In order to see this effect in

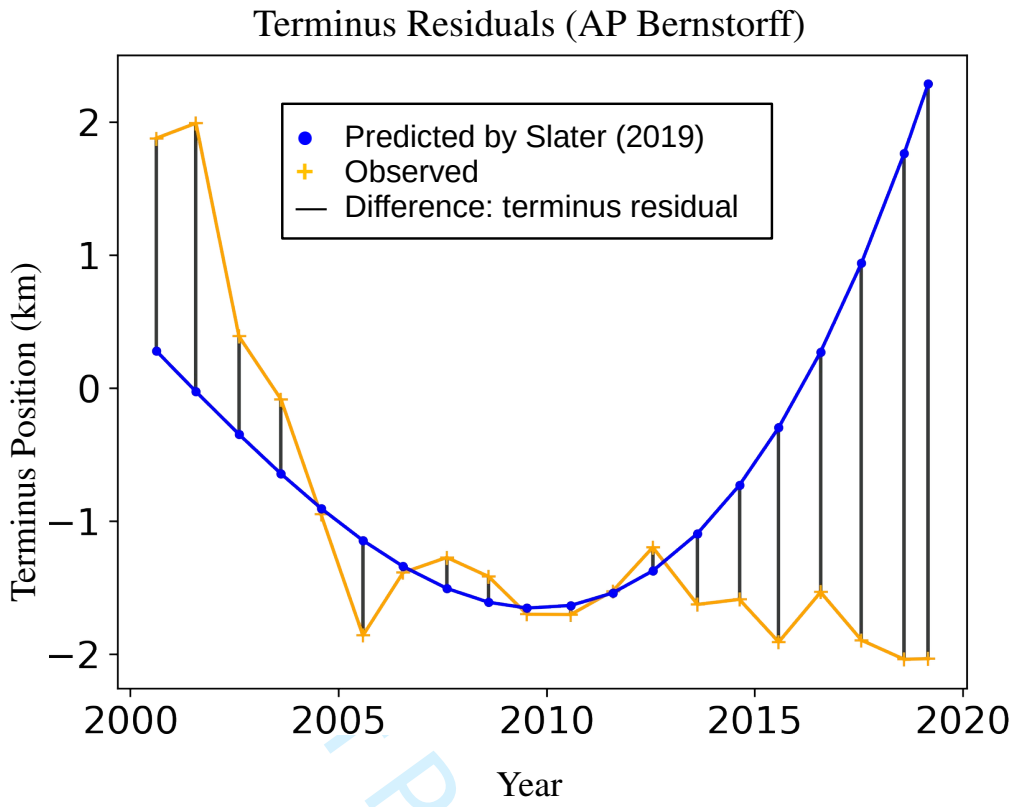

Fig. 7. Computation of the *terminus residual* for AP Bernstorff glacier. **Blue dots:** terminus positions as predicted by thermal forcing model from Slater and others (2019). Annual predictions are available because annual thermal forcing estimates are available; however, note that the Slater model coefficients are determined based on regressions involving 5-year averaged data. **Orange plusses:** terminus positions based on *up area* calculated from termini in Wood and others (2021) and calibrated to terminus positions from Slater and others (2019). **Black lines:** The terminus residual is the difference between the two predictions. The increasingly negative terminus residual means the glacier is retreating faster than Slater and others (2019) would predict based on thermal forcing alone, indicating a destabilizing influence of fjord geometry. The *Fjord Map* for this glacier (Figure 17) confirms that runaway retreat is well underweay.

the data, it is essential to remove the dominant effect of ocean warming. This takes place in two steps: calibration and computation.

Calibration and Computation

This study describes observed terminus state based on data from Wood and others (2021) using *up area* A_T (Section 3.2); whereas Slater and others (2019) describes observed terminus state as a linear position l_s along a center line. Assuming a constant fjord width w, there is a linear relationship between the two:

$$A_T = w l_s + b. \tag{3}$$

We determine w and b empirically via linear linear regression, where b is an arbitrary constant that depends on zero points chosen for l_s and A_T. These coefficients are then used to convert observed *up area* A_T to observed l_w, an effective terminus position calibrated to the same scale and offset used in Slater and others (2019):

$$l_w = (A_T - b)/w. \tag{4}$$

Using Equations 2 and 4, the predicted terminus position l_p (Slater and others, 2019) *based solely on observed advection vs increases in frontal melt due to ocean warming* may be compared to the observed terminus position l_w, which is based on all processes affecting terminus position (Equation 1). We compute the *terminus residual* l_ϵ (Figure 7) as:

$$l_\epsilon = l_p - l_w = \kappa q_m + \beta - \frac{A_T - b}{w}. \tag{5}$$

l_ϵ will be affected by all processes *except* advection and frontal melt: calving (q_c) and thinning-induced retreat (q_s). The supplement from Wood and others (2021) shows that q_s is at least an order of magnitude smaller than q_c for these glaciers. Therefore to first order, l_ϵ is an estimate of advance or retreat due to decreases or increases in calving.

Observations show that some glaciers have been stable, for example *Rink Isbræ* and *Sermeq Avannarleq* (Figure 16). Even though they have been stable overall, their termini have still advanced or retreated by up to 600 m over the study period; where total retreat is computed based on a least squares fit through the annual terminus locations. Therefore, total retreat of less than 600 m over the study period of 1980–2020 is considered not significant because that is within the common range of natural variability for stable glaciers in this study, and the terminus has had little opportunity to "sample" different portions of the fjord. Note that most glaciers in our study that are retreating today only began to do so around the year 2000 (Murray and others, 2015).

4. CLASSIFICATON BY TGC STAGE

The current stage in the TGC for an individual glacier may be evaluated by computing the calving proxy $\bar{\sigma_T}$ and regressing it against the terminus residuals (Section 3.3). Derivation of $\bar{\sigma_T}$, based on the von Mises Calving Law, follows below.

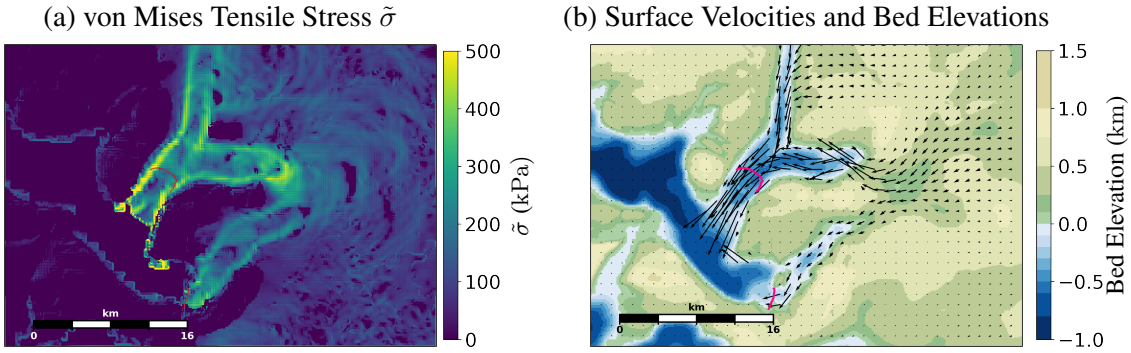

Fig. 8. (a) von Mises tensile stress $\tilde{\sigma}$ shown for Kangilleq and Sermeq Silarleq, as computed by the *Parallel Ice Sheet Model* (PISM), based on a sample velocity field from 2018. (b) Ice velocity vectors and sample terminus (red line), used in conjunction with $\tilde{\sigma}$ to obtain calving proxy σ_T. Ice velocities downstream of the terminus do not reflect grounded ice, they could be an ice shelf or ice melange.

4.1. von Mises Calving Law

The von Mises Calving Law (von Mises, 1913; Morlighem and others, 2016) predicts a glacier will calve when the tensile von Mises stress $\tilde{\sigma}$ at the terminus exceeds the ice's yield strength σ_{max}. The calving rate q_c is given by Morlighem and others (2016):

$$q_c = \frac{\tilde{\sigma}}{\sigma_{max}} ||\vec{u}||, \tag{6}$$

where $\vec{u}$ is the vertically-averaged horizontal velocity. We assume plug flow near the calving front (Bassis and Ultee, 2019; Greve and Blatter, 2009), making the vertically averaged velocity equal to surface velocity.

4.2. Tensile von Mises Stress

The von Mises Calving Law requires computation of the *tensile von Mises stress*. In continuum mechanics, the strain rate tensor $\dot{\epsilon}$ may be computed from the gradient of the velocity $\vec{u}$ as:

$$\dot{\epsilon} = \frac{1}{2}\left(\nabla\vec{u} + \nabla\vec{u}^T\right), \tag{7}$$

where $\nabla\vec{u}^T$ is the transpose of the rank 2 tensor $\nabla\vec{u}$; see Gibbs and Wilson (1901) page 404 Eq 3, also Cajori (1928) volume II page 135. The scalar *tensile strain rate* $\bar{\dot{\epsilon}}$ (Morlighem and others, 2016) is defined as:

$$\bar{\dot{\epsilon}}^2 = \frac{1}{2}\left(\max(0,\dot{\epsilon}_1)^2 + \max(0,\dot{\epsilon}_2)^2\right), \tag{8}$$

where $\dot{\epsilon}_1$ and $\dot{\epsilon}_2$ are the eigenvalues of $\dot{\epsilon}$. Glen's Flow Law, the constitutive relation used to model ice deformation and flow, relates the *strain rate* tensor $\dot{\epsilon}$ to the *deviatoric* or *shear stress* tensor σ:

$$\dot{\epsilon} = \tilde{A}\sigma^n, \tag{9}$$

where $\tilde{A}$ is the temperature-dependant rate factor with units $\mathrm{s}^{-1}\mathrm{Pa}^{-\mathrm{n}}$, and n is typically assumed to be 3 (Behn and others, 2021). In this case (Morlighem and others, 2016), Glen's Flow Law is used with the scalar tensile strain rate $\bar{\dot{\epsilon}}$, and solved for the scalar tensile von Mises stress $\tilde{\sigma}$, to obtain:

$$\tilde{\sigma} = \sqrt{3}\tilde{B}\sqrt[n]{\bar{\dot{\epsilon}}}, \tag{10}$$

where $\tilde{B} = \tilde{A}^{-1/n}$ is the ice hardness (Greve and Blatter, 2009).

Figure 8 shows the von Mises stress computed on a grid for one velocity field. Disregarding processes other than calving for now, the von Mises calving law predicts that advancing glaciers will have $\tilde{\sigma} < \sigma_{max}$, and retreating glaciers will have $\tilde{\sigma} > \sigma_{max}$. As a catch-all parameter, σ_{max} accounts not just for ice cliff properties and fjord geometry but all factors affecting calving, for example frozen melange in the fjord (Schlemm and Levermann, 2020).

4.3. Computing von Mises Stress

For each surface velocity map, we use the Parallel Ice Sheet Model (PISM; Khroulev and the PISM Authors, 2022) to compute the tensile von Mises stress $\tilde{\sigma}$ for a given ITS-LIVE velocity field, using the PISM default constant ice hardness of $\tilde{B} = 68\,082\,\mathrm{Pa\,s}^{1/3}$.

4.4. Integrating Across the Terminus

To obtain a single von Mises stress number for a glacier, the von Mises map computed in Section 4.3 is integrated across the glacier's terminus. The value $\sigma_{_T}$ is defined as the average von Mises stress across the glacier terminus for an entire terminus line T of arbitrary shape:

$$\sigma_{_T} = \frac{\int_T (\tilde{\sigma}\vec{u}\cdot\vec{n})ds}{\int_T (\vec{u}\cdot\vec{n})ds}, \tag{11}$$

where $\vec{n}$ is the unit normal and ds is used for the line integral along L, using a rasterized terminus and a raster-based formulation for the line integral (Appendix A).

This definition of $\sigma_{_T}$ is robust to missing velocity data near the edges of fast glacier flow and near the terminus, a common situation when using InSAR data. If $\vec{u}$ is missing at some points along L, then the

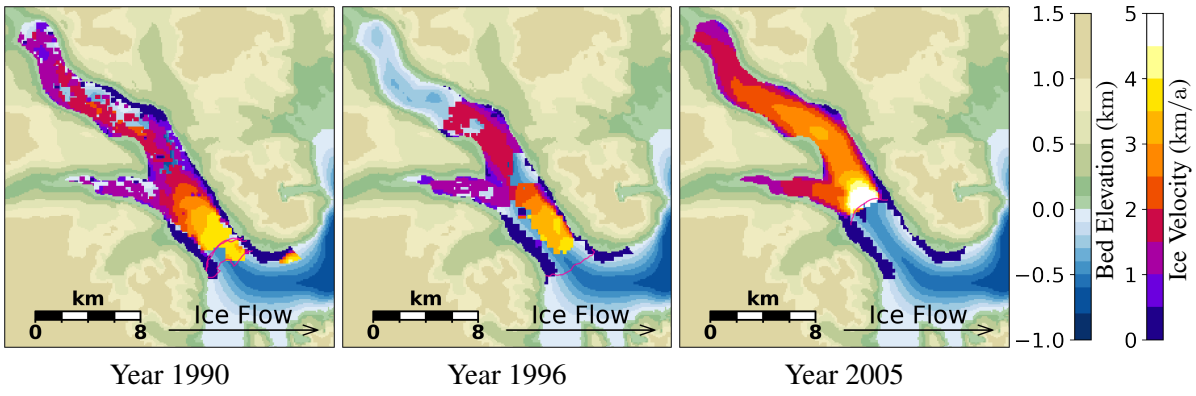

Fig. 9. Aerial map of AP Bernstorff Glacier in Southeast Greenland showing incomplete data for ice velocities that happen in some cases. Annual average InSAR-derived ice velocity data within the fjord are overlaid on bedmap elevation and fjord bathymetry. Ice velocity data are not shown outside the fjord, where bedrock is above sea level. Terminus measurements within the year are shown in red, with three termini available in year 1990, and just one each in 1996 and 2005. Velocity data coverage is sometimes incomplete, especially close to the terminus or near the margins of the glacial trough. Line integrals in this study disregard any portion of the terminus with missing data. Although the equation for σ_T is robust to missing data at the terminus, it can still fail for lack of data, as in 1996.

line integrals in the numerator and denominator will both be missing at the same points along L, and will therefore avoid biasing the result to first order. In this way, σ_T is normalized by the amount of data that can be measured (Figure 9). Because of missing data near the margins, the value of σ_T depends more heavily on what is happening in the center of the fjord.

Annual terminus lines from Wood and others (2021), manually digitized from LANDSAT 5, 7 and 8 imagery, were rasterized on the MEaSUREs grids and used for this analysis. By reusing data from Wood and others (2021), this study maximizes the ability to compare results with other recent work; however, it is also limited to glaciers included in that study.

In theory a one dimensional calving rate q_c can be estimated directly by using σ_T for $\tilde{\sigma}$ in Equation 6. However, errors in estimating σ_{max} lead to large uncertainties in the actual value of q_c, which is not needed anyway. Instead, the von Mises calving law suggests that σ_T on average should be proportional to calving rate q_c. Even without knowing the coefficient of proportionality, this allows σ_T to be used as a proxy for q_c without ever having to explicitly determine σ_{max}.

4.5. Averaging over Velocity Year

Change in surface velocity, not terminus position, is the dominant driver of annual variation in σ_T (Figure 10). To single out the effect of the *position of the terminus in the fjord* rather than surface velocity,

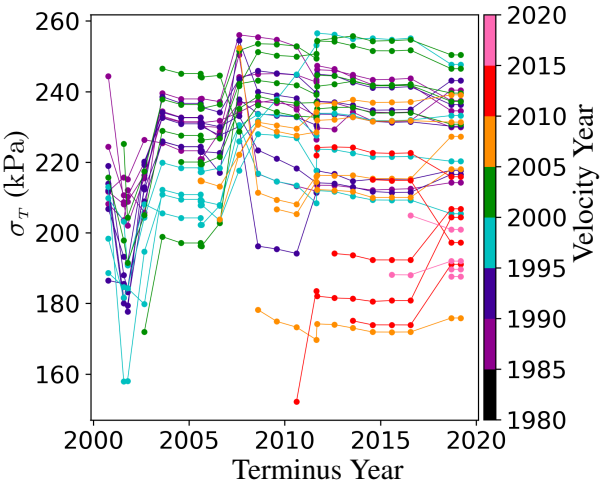

Fig. 10. The calving proxy σ_T value computed for one Glacier (Hayes N); plotted by *velocity year* (year of the velocity field used) and *terminus year* (year of the terminus used), where the velocity year is always less than the terminus year. Although σ_T varies due to the position of the terminus, the largest variation usually occurs due to changes in the overall ice velocity field: some years a glacier may be moving faster, whereas other years it may be moving more slowly. σ_T is averaged across velocity fields of different years to obtain a single value $\bar{\sigma_T}$ for each year's terminus.

σ_T is computed using multiple velocity fields for each terminus, even if the terminus and velocity field are from different years. The result is then averaged to create $\bar{\sigma_T}$. For this procedure to work, there must be ice at the terminus so that σ_T can be computed; which for retreating glaciers means the velocity field must pre-date the terminus position.

Most glaciers in this study were relatively stable until around the year 2000, after which they began to retreat en masse (Murray and others, 2015). Due to limited availability of data and the need for surface velocities to pre-date terminus positions, only the post-2000 period of retreat is studied. Therefore, only terminus/velocity pairs were used in which the terminus year was 2001 or later, and the velocity year was older than the terminus year.

4.6. Effect of InSAR Data Quality

This study uses many approaches to be robust in the face of missing InSAR data. It uses a robust integration technique along the terminus (Section 4.4), and then it uses an averaging technique analogous to *stacking* (Section 4.5), a well established technique in seismology to improve the signal-to-noise ratio of data. Each terminus line is used to integrate all the available velocity fields older than it, thereby decreasing the effect of a poor velocity field on any single year. Figure 10 shows each terminus behaving similarly no matter

which velocity field it is applied to, thereby adding confidence that poor quality velocity fields with missing data are not overwhelming the signal. Finally, termini are only applied to *older* velocity fields. Because most glaciers are retreating, this means that the newer terminus will typically be somewhat upstream of the end of an older velocity field and will likely be sampling an improved portion of that velocity field.

4.7. Analysis of $\bar{\sigma}_T$ and Terminus Residual

The residual l_ϵ represents the amount of terminus advance / retreat that is *not explained* by thermal forcing alone (Section 3.3). With l_ϵ and $\bar{\sigma}_T$ it is now possible to evaluate whether the calving rate proxy $\bar{\sigma}_T$ increases or decreases as the glacier retreats. l_ϵ and $\bar{\sigma}_T$ are regressed against each other wth a p-value significance threshold of 0.21 (see Section **??**):

$$\Delta l_\epsilon = \nu \Delta \bar{\sigma}_T, \tag{12}$$

where ν is the regression coefficient indicating whether fjord geometry causes $\bar{\sigma}_T$ to increase or decrease as the glacier retreats.

If a glacier is susceptible to rapid retreat and has just begun to retreat — as many may be at this point — then the TGC predicts ν should be negative. That is, stress at the terminus $\bar{\sigma}_T$ increases as the glacier begins to retreat, causing a positive feedback that could lead to instability. Such a glacier could well continue to retreat, even if frontal melt rate were to stabilize or decrease.

If on the other hand a glacier is in a stable configuration, then ν will be positive, meaning $\bar{\sigma}_T$ *decreases* as the glacier retreats. Such glaciers could be retreating in spite of their geometric stability due to the primary forcing from warming oceans; however, at this time the fjord geometry is helping stabilize the glacier and prevent runaway retreat.

If a glacier has already begun rapid retreat and is currently retreating through an area with little variation in fjord cross-sectional geometry, then $\bar{\sigma}_T$ will be about constant, even as l_ϵ changes. There is no relationship between $\bar{\sigma}_T$ and the terminus residual l_ϵ, and hence the p-value value for ν will be high. Lack of statistical significance is correlated with glaciers already in rapid retreat, as was confirmed in our results. Note that in principle, lack of predictive power of the Slater regression must also be considered as a possible cause.

5. VALIDATION OF VON MISES CALVING LAW

The von Mises Calving Law as a model may be validated by applying it to the data of Wood and others (2021) and evaluating the result for coherence and consistency. Wood and others (2021) measure or model

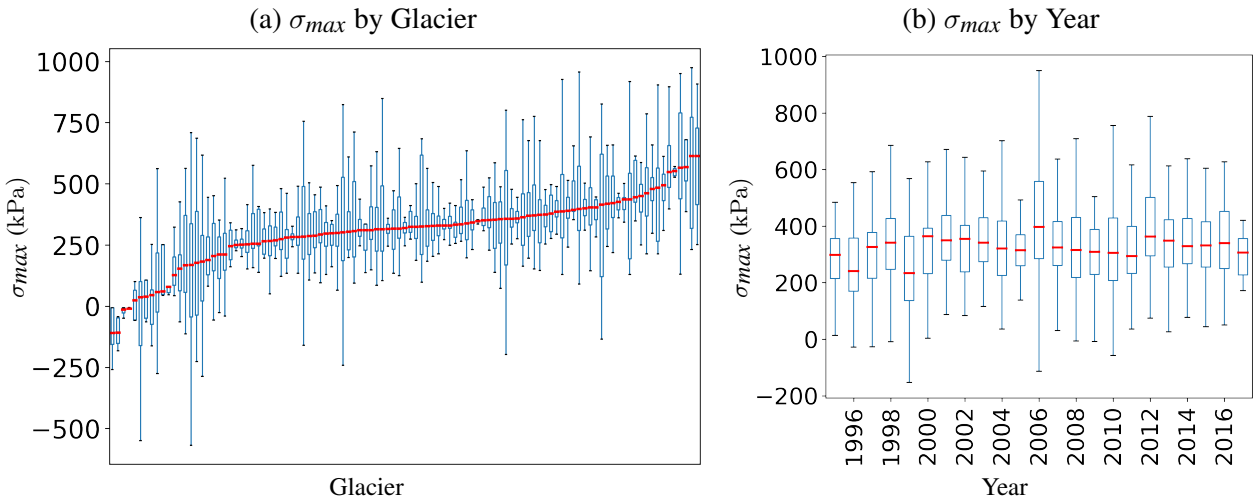

Fig. 11. Implied σ_{max} parameter obtained by fitting σ_τ computed using same-year velocity and terminus measurements, to calving rate obtained by residuals of other quantities from Wood and others (2021) (Equation 13), and grouped by either glacier or year. The red line is the median, the box extends to the edge of the first and third quartile, the whiskers extend to the furthest data point in the first and third quartiles, and outliers are not shown. (a) σ_{max} grouped by glacier. For most glaciers, σ_{max} lies in the range 250 kPa to 350 kPa, with some outliers. Occasional negative values of σ_{max} are non-physical and caused by issues with Wood et al data: σ_τ is always positive. Consistent value across most glaciers supports von Mises calving law as a reasonable model. (b) σ_{max} across all glaciers grouped by year. Consistent year-to-year stability supports von Mises calving law as a reasonable model.

all terms of the mass balance equation (Equation 1) except for the calving rate q_c — which is computed as a residual between observed terminus location L and the integrated effect of all other fluxes: ice advection ($q_f = ||\vec{u}||$), frontal melt (q_m) and thinning-induced retreat (q_s). Although σ_{max} does not need to be computed for this study, it may still be determined from the Wood and others (2021) data and the definition of the von Mises calving law (Equation 6):

$$\sigma_{max} = \frac{\sigma_\tau}{q_c}\frac{dL}{dt}, \tag{13}$$

where dL/dt is the rate of terminus advance or retreat.

Using this formula, σ_{max} was estimated based on all available terminus lines of Wood and others (2021), using the velocity field from the same year as each terminus line. Figure 11(a) shows the result grouped by glacier. In this plot, σ_{max} displays a two-tailed cumulative distribution function. This is to be expected for a value like σ_{max} that is thought to be affected by a number of glacier-specific parameters such as ice shelves, melange characteristics, etc; and would therefore be expected to converge on a normal distribution. Figure 11(b) shows that the average of σ_{max} across all glaciers does not change much from year to year.

These results are reasonable and coherent, even though q_c is a residual, and therefore incorporates all errors and biases from the various datasets and models used by Wood and others (2021). Overall estimated value for σ_{max} is 300 ± 100kPa.

In some cases, σ_{max} is estimated to be negative. That is a limitation of the Wood et al dataset and the nature of q_c as a residual, since σ_τ used in Equation 13 by definition is always positive. The overall consistency of σ_{max} suggests that the von Mises calving law is a useful model for Greenland tidewater glaciers; and that residual values of q_c (Wood and others, 2021) are not overwhelmed by noise, in spite of the multi-step process used to compute them.

Overall, our results (Figure 11) support the von Mises criterion as a reasonable calving model for Greenland tidewater glaciers.

6. RESULTS AND DISCUSSION

Of the 44 glaciers analyzed, 10 were determined to have a destabilizing fjord geometry (the glacier is calving more as it retreats), 7 a stabilizing fjord geometry (the glacier is calving less as it retreats), 16 were found to be stable so far (their termini haven't moved much in the dataset) and 11 to have already entered the rapid retreat phase of the TGC (Figure 12 and 5). Each category is analyzed further below.

6.1. Destabilizing Fjord Geometry

Some glaciers have a regression coefficient $\nu < 0$ (negative slope of line in column (b)), suggesting that they are entering the rapid retreat stage of the TGC. Their termini have retreated substantially (more than 600 m) since 2000; and they have retreated faster than thermal forcing would have predicted.

Puisortoq N and *Puisortoq S* (Figure 14) in Southeast Greenland are both canonical examples of retreat that has continued due to fjord geometry in spite of recent decreases in thermal forcing, suggesting that the retreat has become self-sustaining. *Carlos Glacier* on the west coast offers a similar story.

Some glaciers show episodic retreat; for example, *Eqip Sermia* on the west coast. In this case, the episodic retreat is correlated to changes in thermal forcing, although it could also be due to pinning points.

6.2. Stabilizing Fjord Geometry

Some glaciers have a stabilizing fjord geometry. A small number is to be expected: to be in this category, a glacier must have stable fjord geometry but still be retreating anyway due to frontal melt, a condition that would happen near the end of the rapid retreat phase.

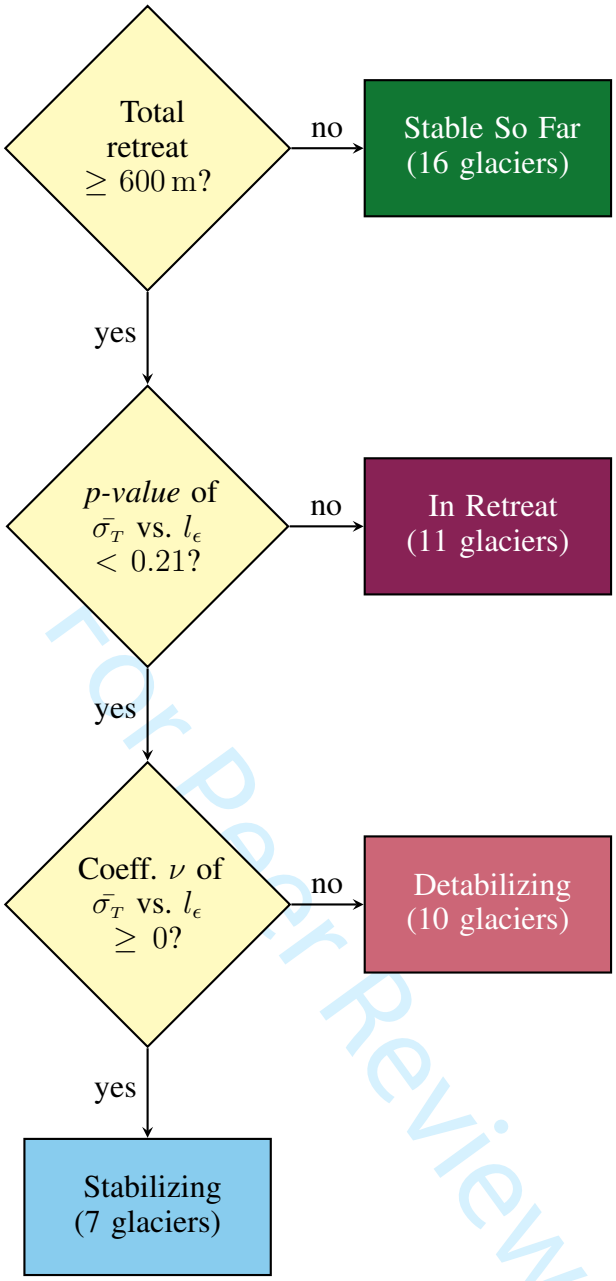

Fig. 12. Glacier categorization flowchart. Glaciers that have moved less than 600 m over the study period are considered stable so far. Otherwise, a regression between the calving proxy $\bar{\sigma_T}$ and the terminus reisdual l_ϵ is performed. If that regression lacks significance at *p-value* of 0.21, then the glacier is considered to already be in rapid retreat. Otherwise, the sign of the regression coefficient ν distinguishes between destabilizing geometery (negative sign) vs. stabilizing geometry (positive sign).

Lille Glacier (Figure 15) is a good example of this, as the terminus retreats into a narrow section at the head of the fjord. *Ussing Braeer N* may also fall into this category, although its geometry is more complex. This increasing stability and slowing down of retreat is the ultimate fate for many tidewater

ID	Name	Latitude	Retreat (m)	ν	p-value	Mean $\bar{\sigma_T}$ (kPa)
			Destablizing			
143	Danell S	E-60.8	-998	-9e-06	0.01	212
85	Puisortoq S	E-61.9	-1762	-2e-05	0.00	264
55	Puisortoq N	E-62.1	-2370	-3e-05	0.00	305
23	Mogens Heinesen S	E-62.4	-2782	-1e-05	0.08	378
90	Eqip Sermia	W-69.8	-2260	-3e-05	0.00	223
52	Kangilernata	W-69.9	-3098	-2e-05	0.21	229
96	Hayes N	W-74.9	-1202	-2e-05	0.01	221
150	Savissuaq WWWW	W-76.2	-3059	-1e-05	0.06	192
89	Docker Smith W	W-76.3	-940	-1e-05	0.07	219
118	Carlos	W-76.4	-806	-7e-06	0.00	212
			Stabilizing			
60	Mogens Heinesen C	E-62.5	-1321	2e-05	0.14	275
10	Uunartit	E-67.4	-4316	5e-05	0.18	322
134	Lille	W-70.5	-814	3e-05	0.02	220
25	Sermeq Silarleq	W-70.8	-4743	3e-05	0.00	304
106	Ussing Braeer N	W-73.9	-688	2e-05	0.00	262
116	Hayes North	W-75.0	-1028	9e-06	0.00	234
192	Savissuaq WW	W-76.3	-1229	8e-06	0.15	167
			Stable			
108	Danell	E-60.9	283	-1e-05	0.10	273
43	Herluf Trolle N	E-61.3	-373	-5e-06	0.03	313
33	Anorituup Kangerlua N	E-61.6	452	1e-06	0.95	386
7	Gyldenlove N	E-64.3	-211	3e-06	0.01	265
14	Koge Bugt S	E-65.0	-283	2e-06	0.57	318
8	Daugaard Jensen	E-71.9	-434	3e-05	0.26	258
36	Kangiata Nunaata	W-64.3	72	-5e-05	0.30	438
13	Kujalleq	W-70.0	-41	7e-06	0.08	408
53	Sermeq Avannarleq	W-70.1	-132	3e-08	0.99	249
6	Store	W-70.4	69	2e-06	0.01	298
119	Sermilik	W-70.6	-14	-2e-07	0.12	223
70	Kangilleq	W-70.7	-24	4e-08	0.85	288
47	Kangerlussuup	W-71.5	-33	-7e-06	0.81	263
5	Rink Isbrae	W-71.7	-139	4e-07	0.81	256
22	Upernavik Isstrom S	W-72.8	-591	-1e-05	0.05	257
24	Hayes M	W-74.8	-20	-5e-06	0.36	301
			In Retreat			
45	Herluf Trolle S	E-61.2	-2359	5e-06	0.31	348
31	Mogens Heinesen N	E-62.5	-3202	-4e-06	0.82	307
12	AP Bernstorff	E-63.8	-2929	3e-05	0.24	263
29	Ikertivaq N	E-65.6	-652	5e-06	0.35	313
2	Kangerlussuaq	E-68.6	-1688	-6e-05	0.28	299
68	Ummiammakku	W-71.7	-5579	-2e-06	0.90	238
88	Inngia	W-72.0	-8038	-7e-05	0.45	156
98	Akullikassaap E	W-73.0	-1915	9e-06	0.78	120
130	Cornell N	W-74.3	-818	-8e-06	0.52	130
37	Hayes NN	W-74.9	-2141	-1e-05	0.33	194
171	Savissuaq WWW	W-76.2	-1663	2e-06	0.37	165

Fig. 13. Summary of results per glacier. Glaciers are grouped by their final categorization (*Destabilizing*, *Stabilizing*, *Stable* or *In Retreat*). Columns are **ID:** ID of glacier as found in Rignot and Mouginot (2012); **Name:** Name of glacier as found in Wood and others (2021); **Latitude:** Latitude (degrees North) of glacier combined with indication of its location on the east (E) or west (W) side of Greenland; **Retreat:** Total amount of retreat (m) over the study period (negative for retreat, positive for advance); $\boldsymbol{\nu}$: Relationship between terminus residuals and $\boldsymbol{\bar{\sigma}_T}$ (Section 4.7); **p-value:** Level of statistical significance of $\boldsymbol{\nu}$ (Section 4.7); **Mean $\boldsymbol{\bar{\sigma}_T}$:** Mean value of $\boldsymbol{\bar{\sigma}_T}$ for this glacier's terminus across *all* years.

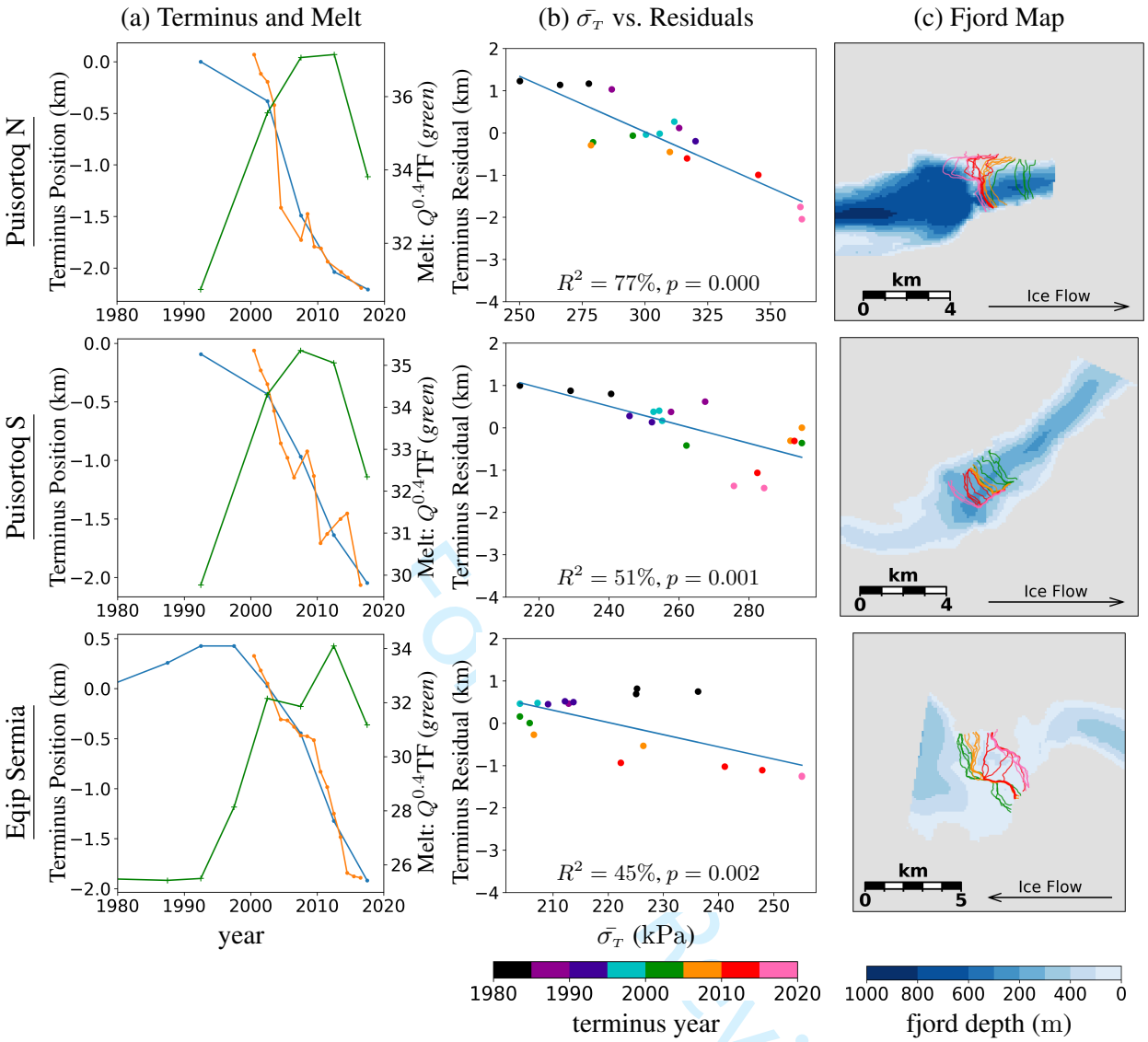

Fig. 14. Analysis of glaciers that destabilize upon retreat. (a) 5-year Slater relative terminus (blue) and melt (green crosses) used in Slater regressions; and annual Wood relative terminus (orange). Slater (blue) and Wood (orange) relative termini should be similar because they measure the same physical quantity. Predictions from the Slater thermal forcing model are not shown. (b) Regression of calving proxy $\bar{\sigma}_T$ vs. relative terminus residuals as per Slater; (c) Reference map of fjord. Although thermal forcing has decreased since 2015, retreat has continued. Based on fjord geometry and recent decreases in retreat rate, Puisortoq N and Eqip Sermia might stabilize soon; however, that is speculation because the terminus has not yet had a chance to "see" these potential pinning points, and thermal forcing could cause continued retreat in any case.

425 glaciers because fjords must become shallower close to their head, or narrower at a pinning point. In the
426 past, glaciers may have come to rest long-term at pinning points, but continually rising ocean temperatures
427 make that less likely in the future. In this study we observe many glaciers slowing their retreat at pinning

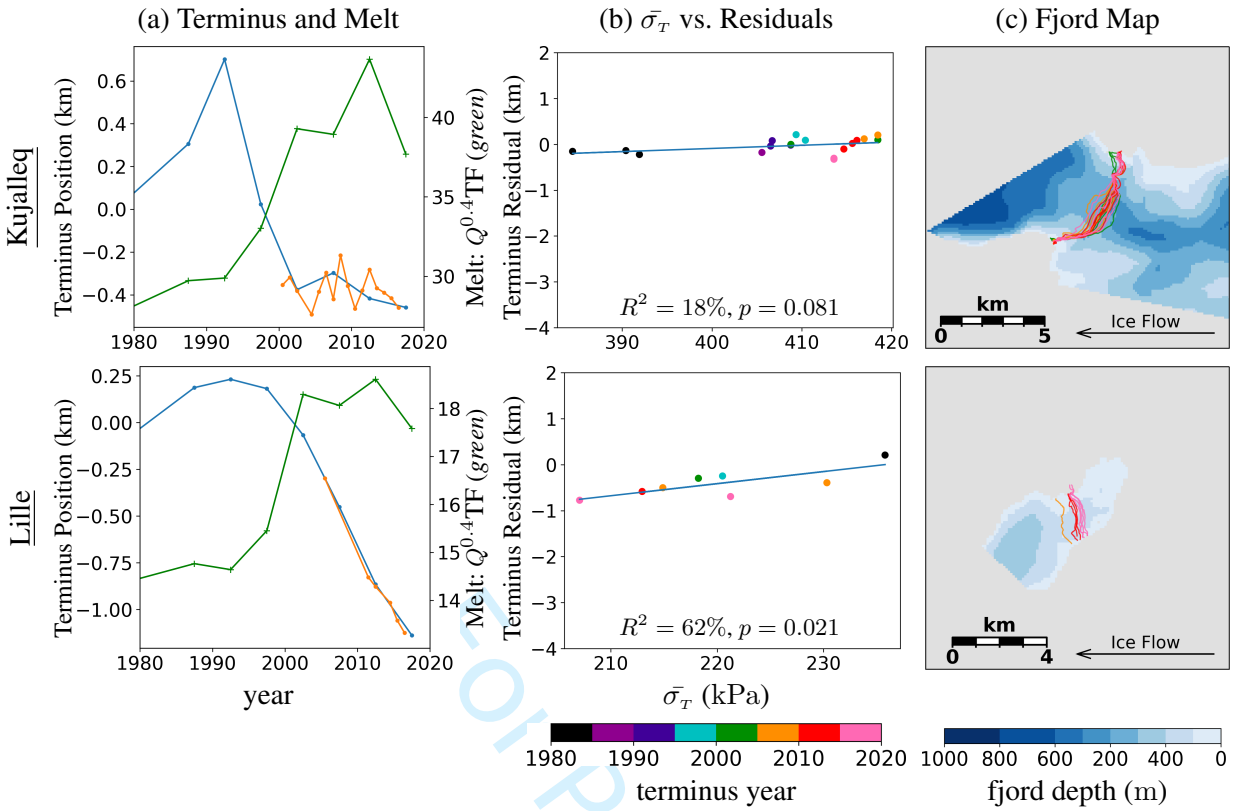

Fig. 15. Analysis of glaciers that stabilize upon retreat. (a) 5-year Slater relative terminus (blue) and melt (green crosses) used in Slater regressions; and annual Wood relative terminus (orange). Slater (blue) and Wood (orange) relative termini should be similar because they measure the same physical quantity. Predictions from the Slater thermal forcing model are not shown. (b) Regression of calving proxy $\bar{\sigma_T}$ vs. relative terminus residuals as per Slater; (c) Reference map of fjord. Gyldenlove N shows two distinct clusters of points — one cluster with unusually low $\bar{\sigma_T}$ and no correlation to residuals, and one cluster with more typical $\bar{\sigma_T}$ values and negative correlation, which would indicate a more typical destabilization upon retreat. The methodology might be confounded here by the complex terminus geometry. Kujalleq's terminus has not moved enough to adequately sample changes in fjord geometry. And from the map, it Lille now terminates near the head of the fjord, where water becomes more shallow with further retreat.

points; but we see no evidence of tidewater glaciers stabilizing anywhere but on land once they have begun rapid retreat.

Some glaciers, for example *Hayes North*, have complex geometry and are a poor "fit" for a linear regression.

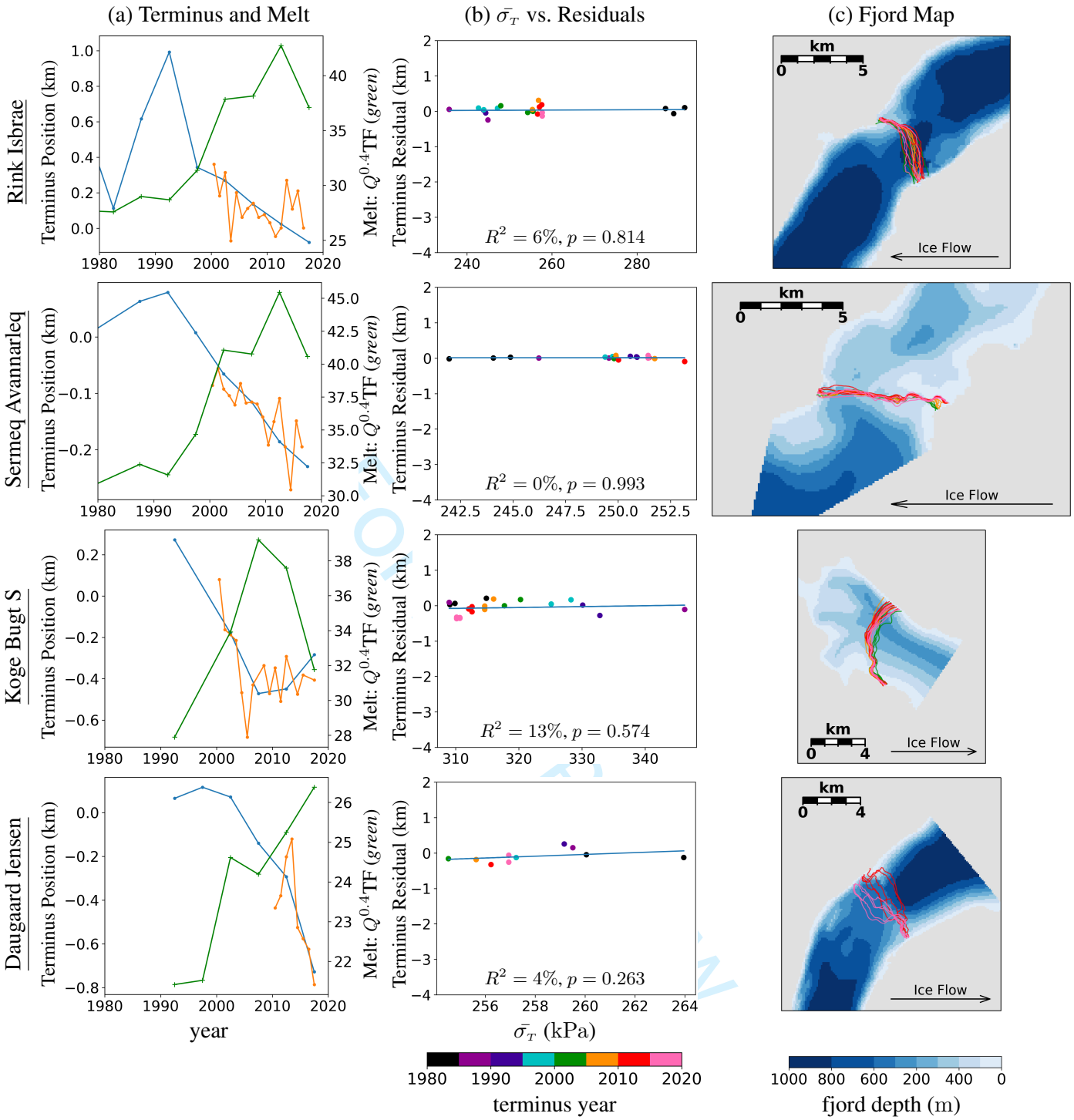

Fig. 16. Analysis of glaciers for which a least square fit of termins position has retreated less than 600 m over the study period; and due to lack of sampling from terminus movement, were statistically insignificant. (a) 5-year Slater relative terminus (blue) and melt (green crosses) used in Slater regressions; and annual Wood relative terminus (orange). Slater (blue) and Wood (orange) relative termini should be similar because they measure the same physical quantity. Predictions from the Slater thermal forcing model are not shown. (b) Regression of calving proxy $\bar{\sigma_T}$ vs. relative terminus residuals as per Slater; (c) Reference map of fjord.

6.3. Currently Stable

Some glaciers have been stable during the study period, with termini that moved on average less than 600 m: the methods of this study revealed no new information about them, beyond their already known recent stability. Because the terminus stayed relatively stationary, no statistically significant relationship was found between terminus residual and $\bar{\sigma}_T$ (Figure 16). The complete list of glaciers in this class is *Anorituup Kangerlua N*, *Daugaard Jensen*, *Hayes M*, *Kangerlussup*, *Kangiata Nunaata*, *Kangilleq*, *Koge Bugt S*, *Rink Isbrae* and *Sermeq Avannarleq*.

To account for noisy data, the threshold for retreat was determined based on the slope of the *least squares fit* line through the terminus positions of Wood and others (2021) since the year 2000. This criterion can yield surprising results in some cases: for example, *Daugaard Jensen*, a glacier that was considered to be "stable" by the criteria of this study. The glacier was historically considerd stable, with concern it could soon destabilize (Bevan and others, 2012). Examination of the data suggests it advanced a modest 700 m before 2013, and since then has retreated almost 1 km . The advance and retreat periods cancel out in this study, but only by chance. *Daugaard Jensen* is no longer, in fact a stable glacier — it is currently retreating. This kind of mischaracterization can happen for any glacier that changes its behavior over the study period.

6.4. In Retreat

Finally, there are the glaciers for which no statistically significant relationship could be found between terminus residual and $\bar{\sigma}_T$, and which have retreated at least 600 m over the study period (Figure 17).

As above, some glaciers show transition between regimes, confounding a single linear model. For example, *AP Bernstorff* retreated rapidly until the year 2005, after which it has remained stable — in spite of changes in thermal forcing both up and down. This is apparently caused by a shallowing of the fjord at the current terminus location. *Herluf Trolle S* and *Mogens Heinesen C* are other examples. *Ummiammakku* retreated rapidly until 2010, at which it stabilized on a pinning point. It is classified as *in retreat* by the systematic methods of this study because most of the data show it retreating: if it has truly stopped retreating, there have not yet been enough years of stability to statistically "overwhelm" the previous years of retreat. Improvements to the methodology that weight recent behavior more strongly might be able to overcome this kind of limitation.

Inngia, *Kangerlussuaq*, *Mogens Heinesen N* and *Savissuaq WWW* are retreating steadily through a uniform portion of the fjord, likely driven by thermal forcing and already "knocked" off their stable terminal

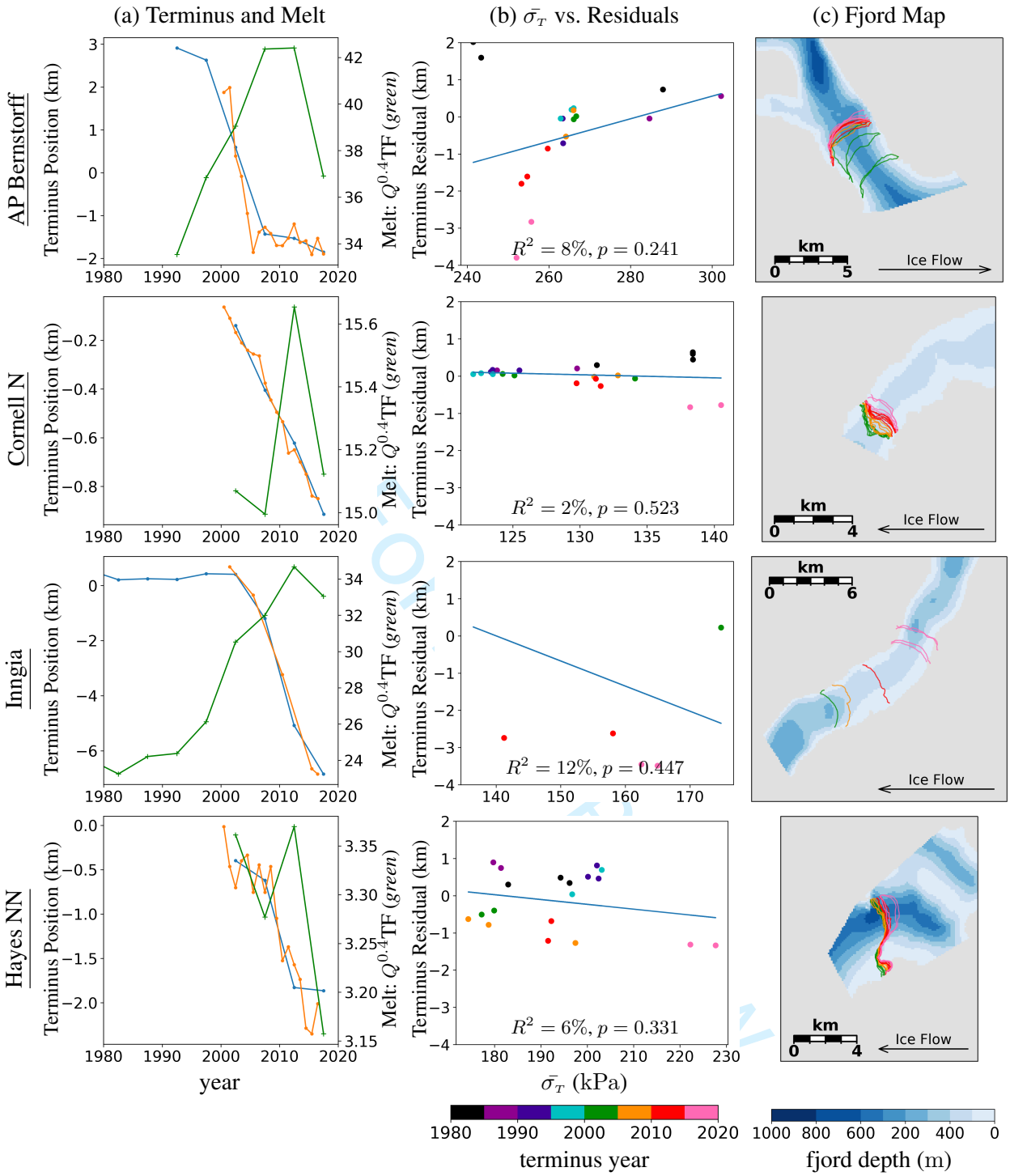

Fig. 17. Analysis of glaciers lacking a statistically significant relationship between $\bar{\sigma_T}$ and relative terminus residual, but with more than 600 m of retreat. (a) 5-year Slater relative terminus (blue) and melt (green crosses) used in Slater regressions; and annual Wood relative terminus (orange). Slater (blue) and Wood (orange) relative termini should be similar because they measure the same physical quantity. Predictions from the Slater thermal forcing model are not shown. (b) Regression of calving proxy $\bar{\sigma_T}$ vs. relative terminus residuals as per Slater; (c) Reference map of fjord. A simple linear regression is confounded for *AP Bernstorff*, which underwent a regime transition around 2005. *Cornell N* has not retreated enough to produce statistically significant results. *Inngia* is in rapid retreat along a homogenous section of the fjord. *Hayes NN* exhibits complex geometry that is hard to describe or classify, with multiple adjacent glaciers and calving fronts.

462 moraine before the start of this study. Fjord geometry does not affect retreat at this point in time because
463 of this uniformity, which results in a "cloud" of points and lack of statistical significance when regressing for
464 ν (the slope of the line in column (b)). However, they all show negative ν at less than statistical significance,
465 suggesting that small variations in fjord geometry *are* affecting terminus position as the TGC hypothesis
466 would suggest.

467 Some glacier termini inhabit broad regions of grounded ice without well defined fjords, often fed by
468 multiple glaciers upstream. In these cases, neither Slater's thermal forcing model nor the Tidewater Glacier
469 Cycle seems to show much predictive power; *Hayes NN* and *Uunartit*, for example. Some glaciers *do* exist
470 in well defined fjords but the terminus is close to a branching or merging point, for example *Savissuaq*
471 *WW*.

472 Other glaciers simply lack data sufficient to build statistically meaningful results: for example, Wood and
473 others (2021) provide only two terminus positions for *Akullikassaap E* and three for *Anorituup Kangerlua*
474 *N*.

475 ## 6.5. Edge Cases

476 The choice of the threshold at 0.21 to separate glaciers in rapid retreat from ones that are stabilizing
477 / destabilizing (Figure 12) is somewhat arbitrary. Some glaciers show clear and consistent behavior and
478 have small p-values, for example *Puisortoq N* (Figure 14) and *Lille* (Figure 15). Other glaciers show large
479 p-values indicating no effect of changes in fjord geometry on continued retreat (Figure 17). However, it is
480 harder to classify the behavior of glaciers with p-values close 0.21.

481 Figure 18 shows the glaciers of highest p-value in each of the *destabilizing* and *stabilizing* categories,
482 and the glacier of lowest p-value in the *in retreat* category (*AP Bernstorff*). All three of these glaciers are
483 correctly classified, but are also edge cases for their categories, as evidenced by their marginal p-values.

484 *Kangilernata* is in fact destabilizing; but it is retreating off an unusually broad shoal more than 2 km
485 wide, creating a situation, similar to that of ongoing rapid retreat, in which the fjord cross section does
486 not change much even as the glacier has retreated more than 2 km.

487 *Uunartit* is in fact stabilizing as it reaches the end of the fjord; but the scenario is confounded because
488 *this* fjord gets deeper even as it narrows, thereby reducing for now the amount that calving decreases
489 as it retreats.

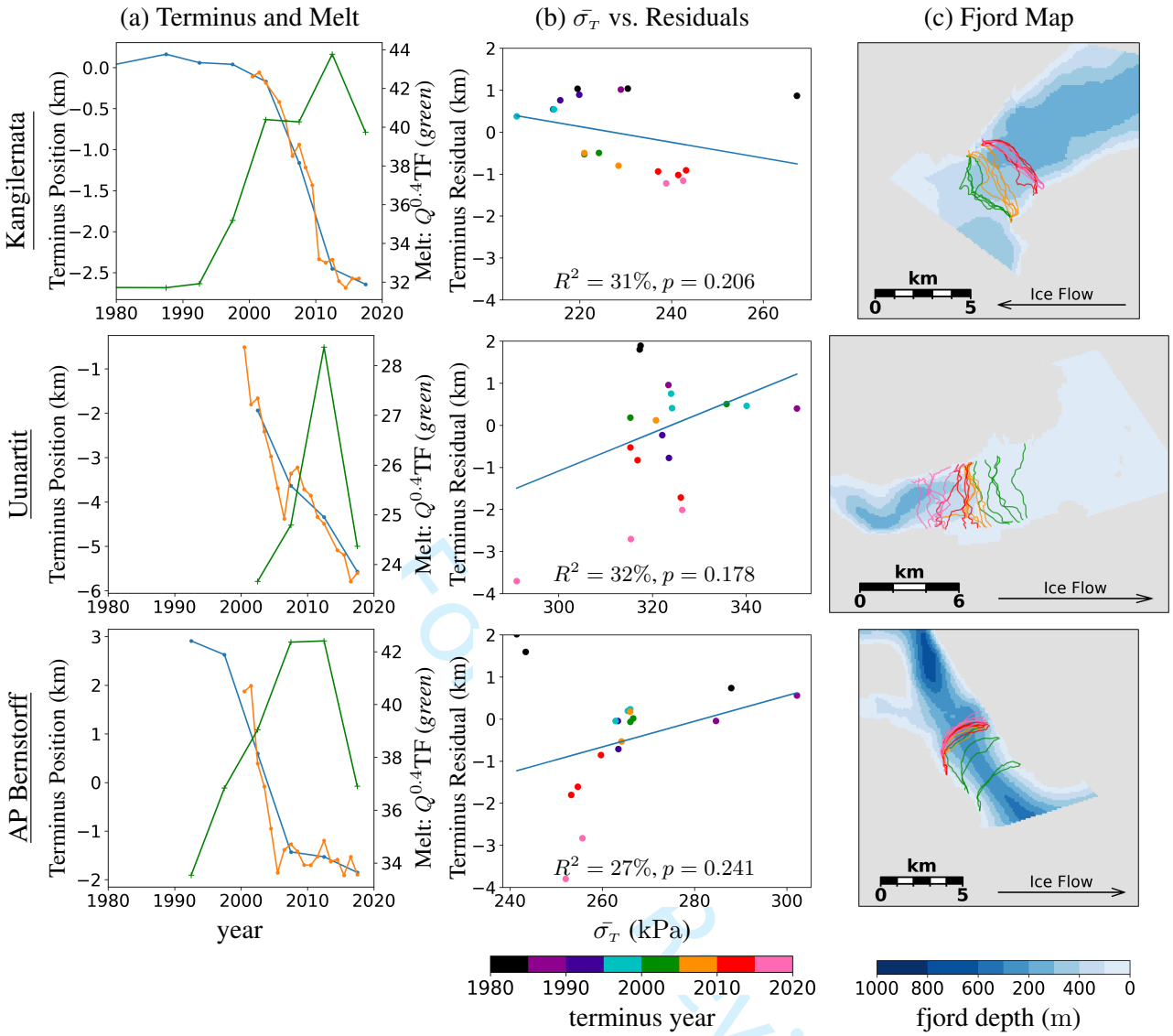

Fig. 18. Edge case glaciers within each category: *Kangilernata* and *Uunartit* are destabilizing and stabilizing, respectively, and have the highest p-values in their classifications. *AP Bernstorff* is in retreat and has the lowest p-value in its classification.

AP Bernstorff is in fact in the midst of rapid retreat; however, retreat has recently slowed down as it has reached a shallower section of the fjord, resulting in overall more stabilizing behavior. This shows how changes in behavior over the study period can confound the methods of this study.

Full results and classifications are provided in the Supplemental material, allowing the reader to compare other glaciers to these edge cases and to evaluate the potential effect of other p-value cutoffs. Although the cutoff value $p = 0.21$ provided accurate classifications in this case, we do not expect $p = 0.21$ to be fundamental to this method. The data sources in this study came with large and often unquantifiable

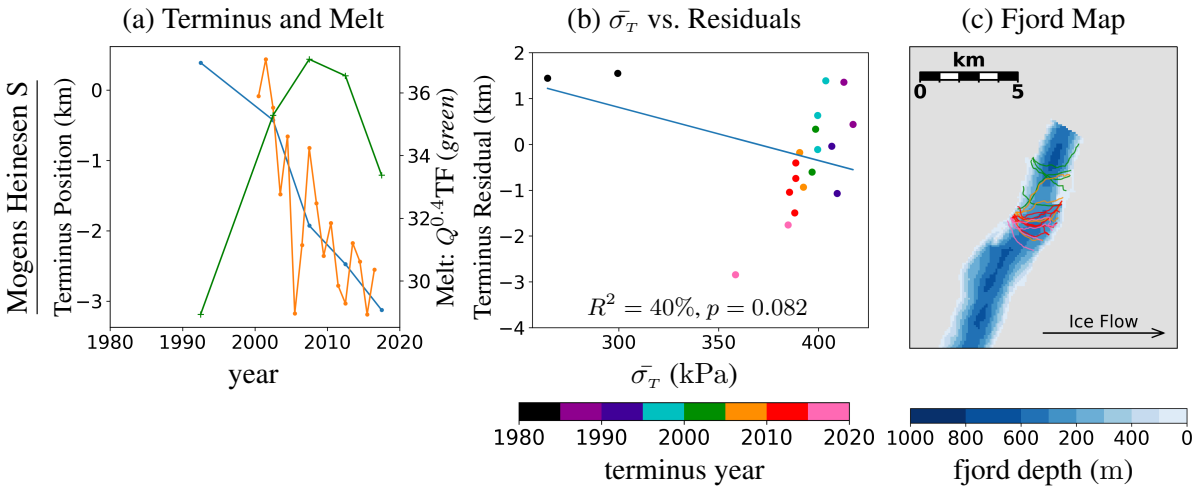

Fig. 19. *Mogens Heinesen S*, which is mis-classified due to two outlier points in the regression of σ_T vs. Residuals (column b).

uncertainties. If those were to be reduced in a future study, we would expect a smaller p-value cutoff to be appropriate.

6.6. Outliers

In some cases, outliers can cause the regression to mis-classify. For example, *Mogens Heinesen S* (Figure 19) is classified as *stabilizing*, but the regression data suggest it is actually *destabilizing*, except for two outlier data points from the 1980's.

7. CONCLUSIONS

This study quantitatively identifies glaciers for which fjord geometry is either adding to or detracting from terminus stability, based on the calving proxy $\bar{\sigma}_T$; and qualitatively matches to expectations based on a visualization of fjord geometry. We draw the following conclusions:

This study provides quantitative support for Tidewater Glacier Cycle as a useful model for understanding the behavior of tidewater glaciers in Greenland, showing general agreement with that model.

This study confirms the general assertions of Wood and others (2021) and Slater and others (2019), concluding that increased frontal melt due to ocean warming since the year 2000 is currently the dominant process driving tidewater glacier retreat in Greenland today. This dominant effect must be removed from the data in order to study calving dynamics and rapid retreat controlled by fjord geometry. Frontal melt has only recently become the dominant mechanism for tidewater glacier retreat

in Greenland. In fact, early work on the tidewater glaciers focus on calving as the primary mechanism of retreat, and does not address ocean warming (Post, 1975; Meier and Post, 1987).

Although statistically significant in many cases, the linear relationship between ocean thermal forcing and tidewater glacier retreat as developed by Slater and others (2019) should be used with caution because it does not account for the calving effects of fjord geometry inherent in the TGC. In the limit, the linear relationship would suggest tidewater glaciers behave like land terminating glaciers, advancing and retreating in lockstep with climate, which runs contrary to our understanding of the TGC (Pfeffer, 2007). For this reason, we suggest caution in using Slater and others (2019) to generate future extrapolated boundary conditions for a GCM, as was proposed in that study.

In spite of increasing frontal melt, not all Greenland glaciers are retreating. One can hypothesize this is due to exceptionally stabilizing fjord geometry, but the methods of this study are unable to confirm or deny such a hypothesis. Speculation on the future of currently stable glaciers might best be accomplished through modeling studies based on the measured bed geometry and idealized thermal forcings and frontal melt.

A number of glaciers confound the methods presented here. Some lack statistical significance for glaciers with complex bed geometries or ill-defined fjords. Some transition between regimes over time — either increasing or decreasing retreat rate quickly as in a surge-type glacier. These issues are problems in the current analysis, which is based on simple linear regressions with an assumption of stationarity. However, the satellite era for glaciers is short and overall lack of data could render useless efforts to use more powerful machine learning techniques, which would require large datasets.

In spite of the complexity, the main thrust of the Tidewater Glacier Cycle is consistently supported by the evidence in this systematic study of glaciers. Glaciers that retreat faster than thermal forcing models would predict have increasing $\bar{\sigma_T}$ with retreat; and in these cases, the terminus is observed to be retreating through a section of the fjord that is widening or deepening, thereby generally confirming the TGC. Whereas glaciers with less retreat than thermal forcing would show decreasing $\bar{\sigma_T}$, which can often be verified by observing pinning points, confirming the TGC as well.

Based on data from Wood and others (2021) and estimates of σ_{max} from that data, this study supports the von Mises criterion as a reasonable calving model for Greenland tidewater glaciers (Figure 11), with $\sigma_{max} \approx 300 \pm 100$kPa.

8. FUTURE WORK

The present study offers encouraging preliminary results that could be improved in many ways: more glaciers in the study, more data per glaciers, more advanced machine learning techniques, and more predictor variables. Lack of data over only 20 years is a persistent issues limiting the statistical techniques available.

Although glaciers are examined systematically in this study, only 44 of the over 200 Greenland tidewater outlet glaciers (Fahrner and others, 2021) were included, a consequence of relying on multiple previous studies for data. The limiting factor was the requirement that glaciers appear in *both* the Wood and Slater datasets, and also on a MEaSUREs grid. Although Wood and others (2021) provide data on the different factors driving terminus retreat, ultimately the only portion of that dataset used was the terminus lines. Recent efforts have produced abundant terminus traces through machine learning techniques (Cheng and others, 2021a), which could in principle allow these methods to be run on more data and a larger set of glaciers. It might be possible to reduce noise by "stacking" results from high frequency terminus measurements from different seasons within one year. Similarly, it might be possible to use more than one velocity field per year.

Improving the data analysis of this study is another avenue for future research. The current study uses two sequential linear regressions: first the regression of Slater and others (2019), and then a regression of $\bar{\sigma_T}$ on terminus residuals. More typically, multiple linear regression would be used here.

The use of sub-annual termini could add data for more robust statistics, but would also introduce more natural seasonal variability in terminus position, which would have to be accounted for; there is no obvious way to take an "average" of multiple terminus lines. Recent efforts have produced abundant terminus traces through machine learning techniques such as automated deep learning (Cheng and others, 2021a), which would in principle enable a larger number of glaciers for a study like this.

Beyond that, the volume of data permitting, advanced machine learning techniques could be applied to predict terminus position based on a range of predictor variables: subsurface runoff (Q), ocean/fjord thermal forcing (TF), $\bar{\sigma_T}$, air temperature, and other climate drivers (Fahrner and others, 2021). These methods might be a reasonable way to use high-frequency (sub-annual) terminus lines and velocity fields.

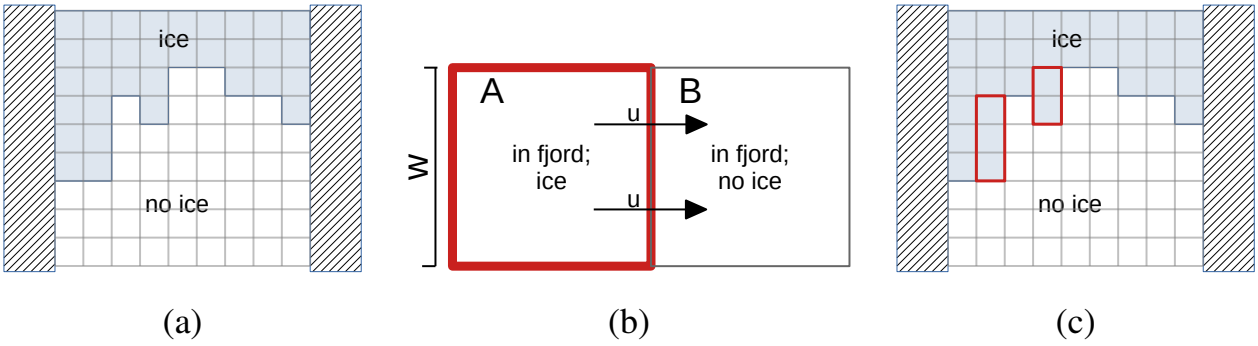

Fig. 20. Illustration of line integrals on a grid. (a) Schematic of gridded ice mask, in which the terminus boundary follows grid cell boundaries; hatched areas are the edge of the fjord. (b) Grid cell A has west-to-east flux flowing into grid cell B, based on the u component of the vector field. Such cells are identified by the rule that A must be in the fjord and ice covered; whereas B must be in the fjord and ice-free. (c) Illustration of grid cells, in red, that have west-to-east flux across the gridded terminus.

The observational methods in this study rely on large amounts of data and are only applicable for the satellite era. For the study of tideater glacier behavior in the past or future, modelling based on dynamic ice models such as PISM (PISM; Khroulev and the PISM Authors, 2022) bounded by *Bed Machine* (Morlighem and others, 2017) would be more appropriate. Although observations from before the satellite era are too sparse to use for the methods in this study, they would be invaluable in calibrating and validating physics based models, opening a window into the past.

Although this study focuses on Greenland only, it does not rely on any properties specific to Greenland; and given appropriate datasets, we believe its methods can be generalized to tidewater glaciers worldwide. Given appropriate data, these methods could help provide a stability assessment for tidewater glaciers in other regions such as Alaska and Antarctica.

APPENDIX A. LINE INTEGRALS ON A GRID

Computation of the *up area* (Section 3.2) provides a gridded *ice mask*, which is used to determine whether each grid cells is ice-covered or ice-free. A vector field is also provided on the same grid (components u and v); for example, representing surface velocity. The method presented here allows line integration of the vector field across the terminus directly on the gridded represenation, without having to convert the termnius to a set of line segments.

The key observation is that in a gridded environment, *the boundary of the ice sheet follows gridcell boundaries*, like a "Manhattan" street grid (Figure 20a) because flux of a constant vector field across a

line depends only on its endpoints. Integrating a vector field across this boundary will produce a result approximately equal to integration of the same vector field across a more physically realistic boundary, which is approximated here in gridded form. Note that the gridded form is "native" to this study, which identifies the *up area* in gridded form. Therefore, flux across the gridded terminus can be broken into four parts, which can be summed together for total flux: flux west-to-east, flux east-to-west, flux north-to-south and flux south-to-north. Without loss of generality, we focus on the west-to-east part of flux.

Suppose a grid cell A on the terminus with ice flowing west-to-east has been identified (Figure 20b). The west-to-east flux from grid cell A to B is exactly the u component of the vector field times the length w of the side of the grid cell through which flux is flowing. The v component of the vector field contributes zero here because it is orthogonal to the boundary being integrated across.

Grid cells with west-to-east flux are easily identified: they are exactly those that are contained in the fjord and are ice-covered; and lie just west of another grid cell also contained in the fjord but with no ice. A mask m for such gridcells can be computed using 2-D array operations of shifting and logical AND, in which m is 1 for grid cells with west-to-east flux, and 0 otherwise. Therefore, the total west-to-east flux for the entire terminus is found by computing muw over each grid cell, and then summing over the entire gridded domain. A similar procedure is used to compute the other three parts of the total flux.

REFERENCES

Adcroft A, Hill C, Campin JM, Marshall J and Heimbach P (2004) Overview of the formulation and numerics of the mit gcm. In *Proceedings of the ECMWF seminar series on Numerical Methods, Recent developments in numerical methods for atmosphere and ocean modelling*, 139–149

Amundson JM (2016) A mass-flux perspective of the tidewater glacier cycle. *Journal of Glaciology*, **62**(231), 82–93 (doi: 10.1017/jog.2016.14)

Bassis J and Ultee L (2019) A thin film viscoplastic theory for calving glaciers: toward a bound on the calving rate of glaciers. *Journal of Geophysical Research: Earth Surface*, **124**(8), 2036–2055 (doi: 10.1029/2019JF005160)

Behn MD, Goldsby DL and Hirth G (2021) The role of grain size evolution in the rheology of ice: Implications for reconciling laboratory creep data and the Glen flow law. *Cryosphere*, **15**(9), 4589–4605, ISSN 19940424 (doi: 10.5194/tc-15-4589-2021)

Bevan SL, Murray T, Luckman AJ, Hanna E and Huybrechts P (2012) Stable dynamics in a greenland tidewater glacier over 26 years despite reported thinning. *Annals of Glaciology*, **53**(60), 241–248 (doi: 10.31 89/2102AoG60A076)

Brinkerhoff D, Truffer M and Aschwanden A (2017) Sediment transport drives tidewater glacier periodicity. *Nat. Commun.*, **8**(1), 90, ISSN 2041-1723 (doi: 10.1038/s41467-017-00095-5)

Cajori F (1928) *A History of Mathematical Notations*. Open Court Pub. Co, Chicago (Available as Dover Edition, 1993)

Carlson AE and 10 others (2017) Recent retreat of columbia glacier, alaska: millennial context. *Geology*, **45**(6), 547–550 (doi: 10.1130/G38479.1)

Catania G and 7 others (2018) Geometric controls on tidewater glacier retreat in central western greenland. *Journal of Geophysical Research: Earth Surface*, **123**(8), 2024–2038 (doi: 10.1029/2017JF004499)

Catania G, Stearns L, Moon T, Enderlin E and Jackson R (2020) Future evolution of greenland's marine-terminating outlet glaciers. *Journal of Geophysical Research: Earth Surface*, **125**(2), e2018JF004873 (doi: 10.1029/2018JF004873)

Cheng D and 6 others (2021a) Calving Front Machine (CALFIN): glacial termini dataset and automated deep learning extraction method for Greenland, 1972–2019. *The Cryosphere*, **15**(3), 1663–1675, ISSN 1994-0424 (doi: 10.5194/tc-15-1663-2021)

Cheng Y, Xia M, Qiao G, Li Y, Hai G and Lv D (2021b) Calving cycle of Ninnis Glacier over the last 60 years. *International Journal of Applied Earth Observation and Geoinformation*, **105**, 102612, ISSN 03032434 (doi: 10.1016/j.jag.2021.102612)

Choi Y, Morlighem M, Wood M and Bondzio JH (2018) Comparison of four calving laws to model Greenland outlet glaciers. *The Cryosphere*, **12**(12), 3735–3746, ISSN 1994-0424 (doi: 10.5194/tc-12-3735-2018)

Fahrner D, Lea JM, Brough S, Mair DW and Abermann J (2021) Linear response of the Greenland ice sheet's tidewater glacier terminus positions to climate. *Journal of Glaciology*, **67**(262), 193–203, ISSN 00221430 (doi: 10.1017/jog.2021.13)

Felikson D and 11 others (2017) Inland thinning on the Greenland ice sheet controlled by outlet glacier geometry. *Nature Geoscience*, (April), ISSN 1752-0894 (doi: 10.1038/ngeo2934)

Gardner AS, Fahnestock MA and Scambos TA (2019) ITS_LIVE Regional Glacier and Ice Sheet Surface Velocities (doi: 10.5067/6II6VW8LLWJ7)

Gibbs JW and Wilson EB (1901) *Vector analysis: A text-book for the use of students of mathematics and physics, founded upon the lectures of j. willard gibbs*. Yale University Press

Goliber S and 10 others (2022) Termpicks: a century of greenland glacier terminus data for use in scientific and machine learning applications. *The Cryosphere*, **16**(8), 3215–3233 (doi: 10.5194/tc-16-3215-2022)

Good SA, Martin MJ and Rayner NA (2013) En4: Quality controlled ocean temperature and salinity profiles and monthly objective analyses with uncertainty estimates. *Journal of Geophysical Research: Oceans*, **118**(12), 6704–6716 (doi: 10.1002/2013JC009067)

Greve R and Blatter H (2009) *Dynamics of Ice Sheets and Glaciers*. Advances in Geophysical and Environmental Mechanics and Mathematics, Springer Berlin Heidelberg, ISBN 9783642034152

Jackson RH and 6 others (2022) The relationship between submarine melt and subglacial discharge from observations at a tidewater glacier. *Journal of Geophysical Research: Oceans*, **127**(10), e2021JC018204 (doi: 10.1029/2021JC018204)

Joughin I, Smith BE, Howat IM, Scambos TA and Moon T (2010) Greenland flow variability from ice-sheet-wide velocity mapping. *J. Glaciol.*, **56**(197), 415–430 (doi: 10.3189/002214310792447734)

Joughin I, E Shean D, E Smith B and Floricioiu D (2020) A decade of variability on Jakobshavn Isbræ: Ocean temperatures pace speed through influence on mélange rigidity. *Cryosphere*, **14**(1), 211–227, ISSN 19940424 (doi: 10.5194/tc-14-211-2020)

Khroulev C and the PISM Authors (2022) PISM, a Parallel Ice Sheet Model (doi: 10.5281/zenodo.1199019)

McNeil C and 7 others (2021) The imminent calving retreat of taku glacier. *Eos, Transactions of the American Geophysical Union*, **102**

Meier MF and Post A (1987) Fast Tidewater Glaciers. *J. Geophys. Res.*, **92**(B9), 9051–9058, ISSN 0148-0227 (doi: 10.1029/JB092iB09p09051)

Mercer JH (1961) The Response of Fjord Glaciers to changes in the Firn Limit. *J. Glaciol.*, **9**(29), 850–858

Morlighem M, Rignot E, Mouginot J, Seroussi H and Larour E (2014) Deeply incised submarine glacial valleys beneath the Greenland ice sheet. *Nat. Geosci.*, **7**(6), 18–22, ISSN 1752-0894 (doi: 10.1038/ngeo2167)

Morlighem M and 6 others (2016) Modeling of Store Gletscher's calving dynamics, West Greenland, in response to ocean thermal forcing. *Geophysical Research Letters*, **43**(6), 2659–2666, ISSN 19448007 (doi: 10.1002/2016GL067695)

Morlighem M and 31 others (2017) BedMachine v3: Complete Bed Topography and Ocean Bathymetry Mapping of Greenland From Multibeam Echo Sounding Combined With Mass Conservation. *Geophys. Res. Lett.*, **44**, 11051–11061, ISSN 00948276 (doi: 10.1002/2017GL074954)

Mouginot J, Rignot E, Scheuchl B and Millan R (2017) Comprehensive Annual Ice Sheet Velocity Mapping Using Landsat-8, Sentinel-1, and RADARSAT-2 Data. *Remote Sensing*, **9**(4), 364, ISSN 2072-4292 (doi: 10.3390/rs9040364)

Murray T and 10 others (2015) Extensive retreat of greenland tidewater glaciers, 2000–2010. *Arctic, antarctic, and alpine research*, **47**(3), 427–447 (doi: 10.1657/AAAR0014-049)

Nick FM, van der Veen CJ and Oerlemans J (2007) Controls on advance of tidewater glaciers: Results from numerical modeling applied to Columbia Glacier. *Journal of Geophysical Research: Earth Surface*, **112**(3), 1–11, ISSN 21699011 (doi: 10.1029/2006JF000551)

683 Noël B and 11 others (2018) Modelling the climate and surface mass balance of polar ice sheets using RACMO2 –
684 Part 1: Greenland (1958–2016). *The Cryosphere*, **12**(3), 811–831, ISSN 1994-0424 (doi: 10.5194/tc-12-811-2018)

685 Pearce DM and 10 others (2022) Greenland tidewater glacier advanced rapidly during era of Norse settlement.
686 *Geology*, **50**(6), 704–709, ISSN 0091-7613 (doi: 10.1130/G49644.1)

687 Pfeffer WT (2003) Tidewater glaciers move at their own pace. *Nature*, **426**(6967), 602, ISSN 00280836 (doi:
688 10.1038/426602a)

689 Pfeffer WT (2007) A simple mechanism for irreversible tidewater glacier retreat. *J. Geophys. Res.*, **112**(F3), 3, ISSN
690 0148-0227 (doi: 10.1029/2006JF000590)

691 Pollard D and DeConto RM (2009) A Coupled Ice-Sheet/Ice-Shelf/Sediment Model Applied to a Marine-Margin
692 Flowline: Forced and Unforced Variations. In *Glacial Sedimentary Processes and Products*, 37–52, Blackwell
693 Publishing Ltd., Oxford, UK (doi: 10.1002/9781444304435.ch4)

694 Post A, O'Neel S, Motyka RJ and Streveler G (2011) A complex relationship between calving glaciers and climate.
695 *Eos, Transactions American Geophysical Union*, **92**(37), 305, ISSN 0096-3941 (doi: 10.1029/2011EO370001)

696 Post AS (1975) Preliminary hydrography and historic terminal changes of Columbia Glacier, Alaska. Technical report,
697 USGS (doi: 10.3133/ofr75491)

698 Rignot E and Mouginot J (2012) Ice flow in Greenland for the International Polar Year 2008-2009. *Geophys. Res.*
699 *Lett.*, **39**(11), ISSN 00948276 (doi: 10.1029/2012GL051634)

700 Rignot E and 12 others (2016) Modeling of ocean-induced ice melt rates of five west Greenland glaciers over the past
701 two decades. *Geophysical Research Letters*, **43**(12), 6374–6382, ISSN 00948276 (doi: 10.1002/2016GL068784)

702 Schlemm T and Levermann A (2020) A simple model of mélange buttressing for calving glaciers. *The Cryosphere*
703 (doi: doi.org/10.5194/tc-2020-50)

704 Slater DA and 6 others (2019) Estimating Greenland tidewater glacier retreat driven by submarine melting.
705 *Cryosphere*, **13**(9), 2489–2509, ISSN 19940424 (doi: 10.5194/tc-13-2489-2019)

706 Sutherland D and 8 others (2019) Direct observations of submarine melt and subsurface geometry at a tidewater
707 glacier. *Science*, **365**(6451), 369–374 (doi: 10.1126/science.aax3528)

708 Taylor LS, Quincey DJ and Smith MW (2022) Evaluation of low-cost raspberry pi sensors for photogrammetry of
709 glacier calving fronts. *Natural Hazards and Earth System Sciences Discussions*, 1–22 (doi: 10.5194/nhess-23-329-
710 2023)

711 Thomas RH and Bentley CR (1978) A model for holocene retreat of the west antarctic ice sheet. *Quat. Res.*, **10**(2),
712 150–170 (doi: 10.1016/0033-5894(78)90098-4)

713 von Mises R (1913) Mechanics of solid bodies in the plastically-deformable state. *Nachrichten von der Gesellschaft*
714 *der Wissenschaften zu Göttingen, Mathematisch-Physikalische Klasse*, **4**, 582–592

715 Walter A, Lüthi MP and Vieli A (2020) Calving event size measurements and statistics of eqip sermia, greenland,
716 from terrestrial radar interferometry. *The Cryosphere*, **14**(3), 1051–1066 (doi: 10.5194/tc-14-1051-2020)
717 Wood M and 16 others (2021) Ocean forcing drives glacier retreat in Greenland. *Science Advances*, **7**(1), eaba7282,
718 ISSN 2375-2548 (doi: 10.1126/sciadv.aba7282)
719 Xu Y, Rignot E, Fenty I, Menemenlis D and Flexas MM (2013) Subaqueous melting of Store Glacier, west Greenland
720 from three-dimensional, high-resolution numerical modeling and ocean observations. *Geophys. Res. Lett.*, **40**(17),
721 4648–4653, ISSN 00948276 (doi: 10.1002/grl.50825)

722 SUPPLEMENTS

723 Code and data for this study are available at the NSF arctic data center under
724 `doi:10.18739/A2ZW18T7N`.

725 Supplement S1 provides results for all glaciers are in this study, sorted by category (Figure 12).

726 ACKNOWLEDGEMENTS

727 Thanks to Mark Fahenstock and Martin Truffer for input and evaluation on the experimental design, and
728 the relevance of the results. Thanks to UAF Glaciers Group for feedback at internal seminars. Thanks
729 to Raf Antwerpen for pre-publication review. Thanks to the four anonymous reviewers whose careful and
730 detailed comments resulted in substantial improvements. This project is funded by NSF Grant PR-1603799.